Electron Precise Sodium Carbaboride Nanocrystals from Molten Salts: Single Sources to Boron Carbides

Simon Delacroix, Fernando Igoa, Yang Song, Yann Le Godec, Cristina Coelho-Diogo, Christel Gervais, Gwenaelle Rousse, David Portehault

Electron precise sodium carbaboride nanocrystals from molten salts: single sources to boron carbides

Simon Delacroix,[1,2] Fernando Igoa,[1,2] Yang Song,[1] Yann Le Godec,[2,*] Cristina Coelho-Diogo,[3] Christel Gervais,[1] Gwenaelle Rousse,[4] David Portehault[1,*]

[1] Sorbonne Université, CNRS, Laboratoire de Chimie de la Matière Condensée de Paris (CMCP), 4 place Jussieu, F-75005, Paris, France

[2] Sorbonne Université, CNRS, MNHN, IRD, Institut de Minéralogie, de Physique des Matériaux et de Cosmochimie (IMPMC), 4 place Jussieu, F-75005, Paris, France

[3] Sorbonne Université, CNRS, Institut des Matériaux de Paris Centre (IMPC), 4 place Jussieu, F-75005, Paris, France

[4] Collège de France, Sorbonne Université, Chimie du Solide et de l'Energie (CSE), 75231 Paris Cedex 05, France

*Corresponding authors:

david.portehault@sorbonne-universite.fr

yann.le_godec@sorbonne-universite.fr

Abstract

Boron-rich solids exhibit specific crystal structures and unique properties, which are only very scarcely addressed in nanoparticles. In this work we address the original inorganic structural chemistry and reactivity of boron-rich nanoparticles, by reporting the first occurence of sodium carbaboride nanocrystals based on the NaB_5C crystal structure. To design these sub-10 nm nano-objects, we use liquid-phase synthesis in molten salts at 900 °C. By combining a set of characterization tools including powder X-ray powder diffraction, transmission electron microscopy, solid state nuclear magnetic resonance coupled to DFT modelling and X-ray photoelectron spectroscopy, we demonstrate that these nanocrystals deviate from the ideal stoichiometry reported for the bulk compound. We suggest that the carbon and sodium contents compensate each other to ensure that the octahedral cluster-based framework is stabilized by fulfilling an electron counting rule. These nanocrystals encompass substituted octahedral covalent structural building units not reported in the related bulk compound. They then shed a new light on the ability of nanoparticles to host wide solid solution ranges in covalent solids and then to yield new solids. We finally show that these nanocrystals are efficient single sources of boron and carbon to form a nanostructured boron carbide, thus paving a way to new nanostructured materials.

Introduction

Inorganic chemistry of boron-rich solids is driven by the trend of boron to build covalent bonds with itself.[1,2] These covalent bonds account for many unique properties, but little is known on their occurrence in nanoparticles and their impact on the nanoparticles properties. Metal hexaborides (**Figure 1, Movie S1**) are built on such bonds that yield a covalent framework made of B_6 octahedral units. Although known for a long time, metal hexaborides (**Figure 1, Movie S1**) have been the focus of renewed interest in recent years. Some of them are well known to exhibit field emission (rare earth hexaborides) and thermoelectric (alkaline earth hexaborides) properties, but new and unexpected behaviors have emerged within the last years: LaB_6 exhibits near-infrared surface plasmon resonance[3] while SmB_6 is a Kondo insulator coupled to a specific conductive surface state,[4] which might be related to topological features.[4] Both examples show the importance of controlling the composition, but also the surface states and the surface-to-volume ratio of metal hexaborides in order to control optical and conduction properties, among others. Nanocrystal design provides interesting perspectives in this respect.

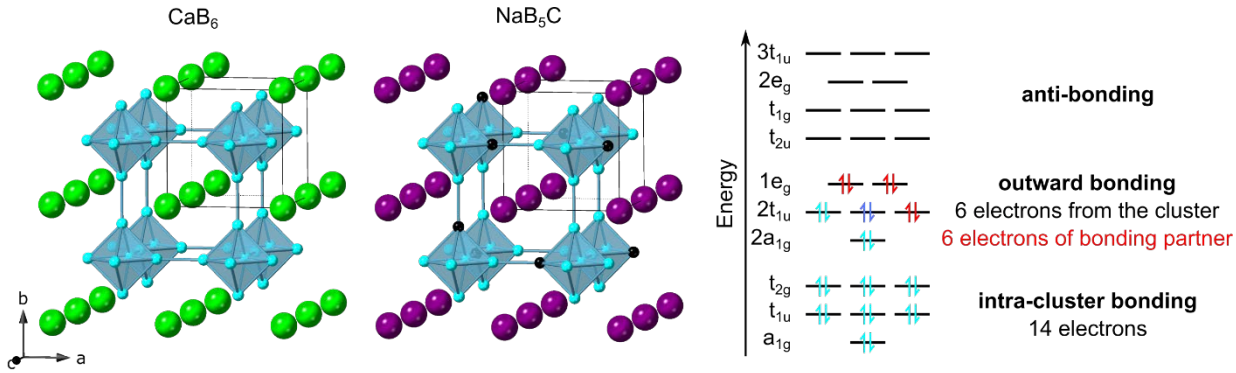

Figure 1. Crystal structures of NaB_5C and CaB_6. Boron, carbon, sodium and calcium atoms are in blue, black, purple and green, respectively. The octahedral clusters are represented in light blue. For NaB_5C, the carbon atoms are placed randomly in each unit cell. The molecular orbital diagram corresponds to one octahedral cluster, analog to the molecular $B_6H_6^{2-}$ anion. Light blue arrows account for electrons provided by 6 boron atoms into a B_6 octahedral cluster. The 6 red arrows correspond to the bonding partners building 6 outward 2center-2electron bonds (B-H bonds in $B_6H_6^{2-}$ analog, inter-cluster B-B bonds in the hexaboride). The remaining 2 blue arrows account for the two additional electrons needed for fully stabilizing the framework.

The theoretical frame explaining the stability and conduction properties of many metal hexaborides has been provided early by Longuet-Higgins and de V. Roberts,[5,6] who have built an analogy between the octahedral B_6 clusters building the hexaboride framework (**Figure 1**) and the $B_6H_6^{2-}$ anion, thus referring to Wade's rules.[7–9] According to the molecular orbital diagram of a B_6 unit (**Figure 1**), the anion reaches a stable closed shell configuration and the B_6 extended framework is stable when each octahedron is provided with 20 electrons. These 20 electrons include 14 electrons filling the intra-octahedron bonding orbitals, and 6 electrons populating each of the 6 outwardly bonding orbitals at each corner of the octahedron to build 2center-2electron inter-octahedra bonds (or B-H bonds for the analog $B_6H_6^{2-}$ anion). The B_6 octahedron provides on itself 18 electrons and the metal encaged between the octahedral units supplies 2 electrons in the formalism of the Zintl concept.[10,11] Overall, with divalent metal cations, like alkaline earth, only the bonding states are filled, which yields semiconductors. In this model, an additional electron, provided with trivalent metal cations would yield metallic compounds, like LaB_6, although more complex effects such as strong electron correlation could change the outcome and yield bulk semiconductors, like SmB_6. In this frame, replacing the metal with an alkali metal supplying only one electron would fail to provide full stabilization, which explains the near complete absence of alkali hexaborides[6] except Li_2B_6[12] and the notable case of metal deficient KB_6, for which a consensus has not been reached.[1,13,14] To go beyond this restriction and in their effort to discover new boron-rich borides of alkali metals, B. Albert and K. Schmitt[15,16] have discovered ternary compounds with the hexaboride structure: alkali carbaborides NaB_5C and KB_5C, which are actually the only carbaborides of sodium and potassium.[1] In these compounds, the B_6 units in hexaborides are replaced by B_5C octahedra. Substituting one boron for one carbon atom in each octahedron provides the missing electron to fulfill the maximal stabilization conditions of the extended octahedral framework.[15,16]

According to this model, one would expect that deviations from the ideal stoichiometry would destabilize the solids. These theoretical considerations have however been difficult to confirm experimentally up to now because of the absence of a local probe for investigating the boron/carbon local environment. On a more fundamental side, given the propensity of nanocrystals to accommodate larger strains and deviations to bulk phase diagrams,[17] the question arises as to whether stoichiometry deviation could occur or be facilitated in alkali carbaboride nanocrystals and if they could host new covalent building units could arise.

In addition, the reactivity of NaB_5C and KB_5C is a virgin field, while other alkali-based compounds of p-block elements are known to exhibit interesting phase transformations when the alkali metal can be eliminated, as in the case of the evolution of sodium silicide Na_4Si_4 to silicon clathrates.[18] A similar chemical evolution for alkali carbaborides could yield boron carbides, of high interest for their hardness[19] and photocatalytic[20] properties. Designing alkali carbaboride nanocrystals would be the key to open a new avenue to nanostructured boron-rich carbides. Again, such a transformation would raise the more general fundamental question of the reactivity of nanoparticles based on covalent bonds.

Addressing the questions of the stoichiometry of alkali carbaboride nanocrystals and of their reactivity requires synthesizing these compounds for the first time as nano-objects, while all previous works have dealt with macroscale crystals formed from the elements, especially strongly inert boron (**Table S1**).[15,16,21,22] The search for a pathway towards alkali carbaboride nanocrystals then sits in the last decade extensive research on the synthesis of metal boride nanoparticles.[23] One of the general routes to reach this aim is the synthesis in molten salts,[24,25] mostly focused on transition metal or rare-earth metal borides[3,26–33] but recently extended to a lithium boride.[34] The method should then be suitable to reach nanocrystals of other alkali-based boron-rich solids, including alkali carbaborides.

In this work, we provide the first occurrence of NaB_5C nanocrystals, by using molten salts as solvent and reagent. The choice of reactive boron and carbon precursors and of liquid-phase reaction provides ideal conditions to trigger fast nucleation of the crystals and then to limit the particle size in the sub-10 nm range. We then use NaB_5C nanocrystals as case-study to address possible deviations from the ideal stoichiometry. We finally show how NaB_5C nanocrystals can be used as single sources of boron and carbon towards boron carbide nanocrystals.

Methods

Sodium borohydride (98 %, Alfa Aesar), sodium iodide (> 99.5 %, Sigma Aldrich), polyethylene (M_w = 35000 g mol^{-1}, Sigma Aldrich), methanol (VWR Normapur grade) were used as received and handled under argon atmosphere in a glovebox (H_2O < 0.5 ppm, O_2 < 0.5 ppm) and with standard Schlenk techniques.

To synthesize NaB_5C, 600 mg of sodium borohydride (15.9 mmol) was grinded with 5 g of sodium iodide and 285 mg of polyethylene (10.2 mmol, C:B atomic ratio of 1:2.75) during two minutes at 20 Hz (Retsch MM400, 50 mL stainless steel bowls filled with one ball) to obtain an homogeneous finely ground powder. The mixture was heated at 900 °C under argon during two hours in a crucible, and then cooled down to room temperature. The synthesis was run in either molybdenum or *h*-BN crucibles. The reaction mixture was washed with methanol by ten cycles of centrifugation and redispersion. The powder was dried under vacuum for 12 h before being stored under argon. 156 mg was typically recovered after synthesis, which corresponds to a yield of 55 % versus the boron precursor. The synthesis was reproduced at least 20 times to ensure reproducibility.

Boron carbide was synthesized by thermal decomposition of sodium carbaboride. The initial powder was placed into a *h*-BN crucible, placed itself into a horizontal tubular oven, which was purged with Ar flow for 1 h before being heated under argon flow up to 1200 °C at a heating rate of 5 °C min^{-1}. Then the temperature was dwelled for 12 h before stopping heating and letting the oven cool down naturally. The resulting powder was washed with methanol by cycles of centrifugation and redispersion until a conductivity of 4 $\mu S \cdot cm^{-1}$ in the supernatant was achieved. The sample was stored in air.

Powder XRD was performed with a Bruker D8 Advance diffractometer in the Bragg-Brentano θ-θ geometry with a CuKα sealed tube X-ray source (λ = 1.5418 Å). Powder patterns were collected in the 2θ range 10-120° with a 0.1° step and collecting data for 20 s/step for NaB_5C, 10-120° with a 0.05° step and 5 s/step for B_4C samples. The reference crystallographic structure of NaB_5C and B_4C were taken from the ICSD database (408930 and 79958 cards, respectively) before being refined according to the Rietveld method using the FullProf Suite software.[35]

XPS spectra were recorded on an Omicron spectrometer using an Al Kα source (1486.7 eV) as the source energy. The binding energies were referenced *versus* the aliphatic C1s peak (284.8 eV).

The specific area was evaluated by applying the BET method to a nitrogen sorption isotherm recorded at 77 K using a BELSORB-max apparatus after degassing the sample at 150 °C for 15 h.

Transmission electron microscopy (TEM) images were acquired with a Technai Spirit 2 microscope operating at 120 kV. The powders were deposited on carbon-coated copper grids by solid-state deposition in an argon glovebox. Energy dispersive X-ray analysis (EDS) was performed on a Hitachi SU-70 scanning electron microscope.

Raman spectroscopy was performed on the powder with a Kaiser Optical System Raman Analyzer RX1 Microprobe with a 785 nm laser diode.

Solid-state MAS NMR spectra were acquired on a Bruker AVANCE III 700 spectrometer (16.4 T magnet) operating at ν_0 = 224.68 and 185.20 MHz for ^{11}B and ^{23}Na respectively and using a 3.2 mm Bruker probe. Powder samples were transferred to ZrO_2 rotors and spun at a MAS rate of 20 kHz. ^{1}H, ^{23}Na and ^{11}B chemical shifts were referenced to TMS, 0.1 M $NaCl_{(aq)}$ and $BF_3 \cdot OEt_2$, respectively.

Different models were obtained starting from the crystalline structure of NaB_5C[16] and using 2×2×2 and 3×3×3 supercells in which carbon atoms were randomly positioned in substitution of one or two borons among B_6 octahedra. In addition, Na vacancies were introduced in some cases as described more precisely later in the text. All atomic positions were then relaxed with the VASP (Vienna Ab-initio Simulation Package) code[36] based on the Kohn-Sham Density Functional Theory (DFT) and using a plane-wave pseudopotential approach. The cells parameters were fixed to X-ray diffraction parameters during geometry optimizations. The NMR parameters were then calculated within the Kohn-Sham DFT using the QUANTUM-ESPRESSO code,[37] keeping the atomic positions equal to the values previously calculated with VASP. The PBE generalized gradient approximation[38] was used and the valence electrons were described by norm conserving pseudopotentials[39] in the Kleinman Bylander form.[40] The shielding tensor was computed using the Gauge Including Projector Augmented Wave (GIPAW) approach,[41] which enables the reproduction of the results of a fully converged all electron calculation. The isotropic chemical shift δ_{iso} is defined as $\delta_{iso} = -[\sigma - \sigma_{ref}]$ where σ is the isotropic shielding and σ_{ref} is the isotropic shielding of the same nucleus in a reference system. In the present case, the comparison between the experimental δ_{iso} and calculated σ_{iso} ^{11}B chemical shift values for B_2O_3 (δ_{iso} = 14.6 ppm) (ICSD reference card 16021) was used for ^{11}B while for ^{23}Na, σ_{ref} was fixed so that the average sum of experimental and

calculated shifts of a series of sodium phosphates and silicates coincide.[42] The principal components V_{xx}, V_{yy}, and V_{zz} of the electric field gradient (EFG) tensor were obtained by diagonalisation of the calculated tensor giving access to the quadrupolar coupling constant C_Q and the asymmetry parameter η_Q, which are defined as : $C_Q = eQV_{zz}/h$ and $\eta_Q = (V_{yy} - V_{xx})/V_{zz}$ (e is the proton charge, h Planck's constant and Q the quadrupole moment of the considered nucleus). The Q value reported by Pyykkö[43] was used in the calculations for ^{11}B (40.5 mb) and ^{23}Na (104 mb). Calculated spectra were then plotted using the DMFit program.[44]

Results and discussion

NaB_5C nanoparticles were synthesized by using sodium borohydride and polyethylene as boron and carbon sources respectively. The reaction was performed at 900 °C in molten sodium iodide (melting point 661 °C), which acted as liquid medium and sodium source. The sample comprises exclusively slightly elongated cubic nanoparticles with a size distribution centered at 7 nm, and edge lengths ranging from 2 to 14 nm (**Figure 2A** and **2B**).

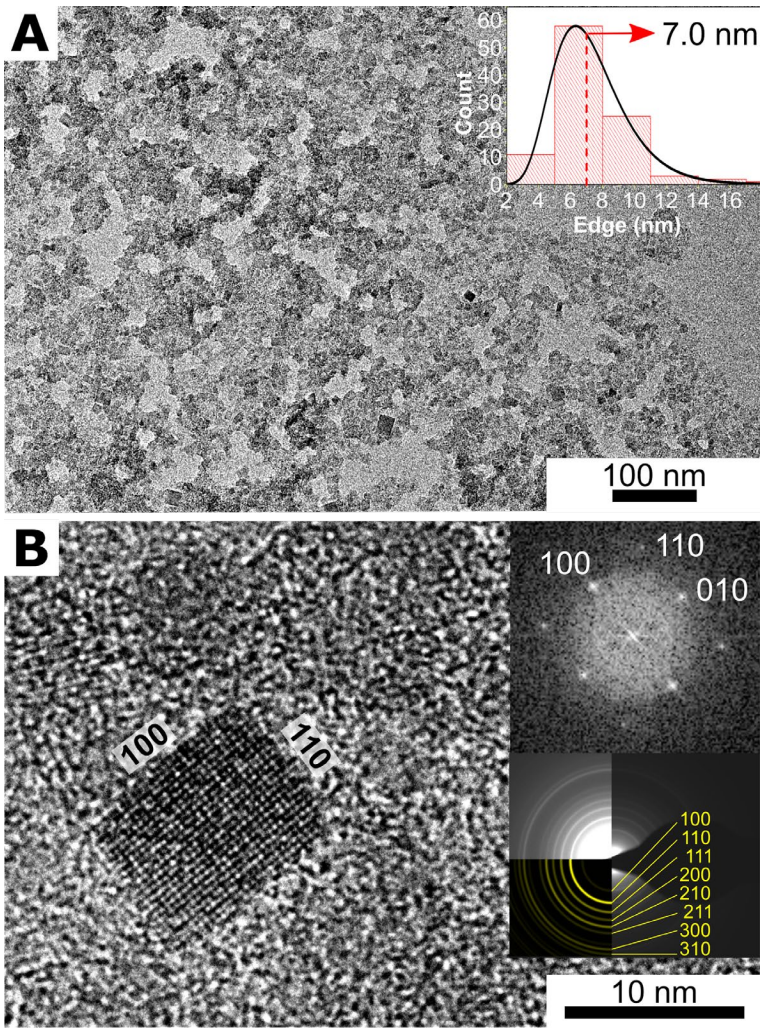

Figure 2. (A) TEM and (B) HRTEM images of NaB_5C-related sodium carbaboride nanocrystals. The corresponding size distribution is shown as inset in (A). The Fast Fourier Transform (FFT) of image (B) is shown as insert, together with the SAED pattern. They are fully indexed along the NaB_5C structure.

The X-ray powder diffraction (XRD) pattern (**Figure 3**) is fully indexed along the cubic Pm-3m space group of the NaB_5C crystal structure. Rietveld refinement with this structure yields for the final model satisfactory conventional figures of merit (R_{wp} = 5.41%, R_B = 0.66%, χ^2 = 6.31). In a first step, the XRD pattern was fitted to the exact NaB_5C stoichiometry (See **Figure S1A-B**).[16] While this model seem appropriate (R_{wp} = 7.42%, R_B = 1.00%, χ^2 = 11.18), discrepancies with the experimental and reported data motivated further analysis. Firstly, the adjustment fails to fully account for the intensity of the (100) reflection at 21.6° (Cu Kα), which represents the largest relative error according to the difference curve. Secondly, the refined cell

parameter – 4.0878(2)Å – is slightly smaller than the reported one of 4.0925(1)Å.[16] We have then refined atomic occupancies in order to further improve the agreement with experimental data. Three approaches were considered: refinement of only the B/C ratio (model I, **Figure S1C-D**), refinement of only the Na occupancy (model II, **Figure S1E-F**) and refinement of both the B/C ratio and the Na occupancy (modle III, **Figure S1G-H**). All three models coincide better with the experimental data (**Figure S1**), since they all influence the pattern by increasing the relative ratio of the (100) reflexion, as compared in **Figure S1** against the (200) and (210) reflexions. However, model I yields a negative B occupancy that is not chemically valid. On the other hand, model II leads to the stoichiometry $Na_{0.809}B_5C$, which deviates from the electron counting rules described above. Model III enables to compensate possible Na vacancies with an increase in the carbon content to fulfill the overall electron counting rule in the B-C framework with 20 electrons per octahedral unit, provided the stoichiometry is restrained to $Na_{1-x}B_{5-x}C_{1+x}$. Accordingly, Rietveld refinement yields the composition of $Na_{0.816}B_{4.816}C_{1.184}$. The results from models II and III are indistinguishable in terms of figures of merit or visual inspection (**Figure S1**). However, model III satisfies the electron counting rule and is then privileged. The solid-state Nuclear Magnetic Resonance (NMR) discussed later further supports this choice. The refinement is clearly in better agreement with the experimental diagram compared to the refinement from the ideal NaB_5C model (**Figure S1**). The bond lengths within and between the clusters are on average 1.74 and 1.63 Å respectively for model III, which is in overall agreement with the reported octahedra-based framework of NaB_5C. The resulting stoichiometry corresponds to molar ratios Na/B and B/C of 0.17 and 4.07, respectively, *versus* 0.20 and 5.00 for the tabulated NaB_5C compound.[16] According to the final Rietveld refinement of the XRD pattern, the crystallite size is 5.0 nm in agreement with the particle size from TEM, suggesting that each nanoparticle consists in a single crystal domain. This is confirmed by High resolution TEM (HRTEM) (**Figure 2B**).

HRTEM is also in agreement with the NaB_5C crystal structure. The NaB_5C nanocrystals expose {100} facets.

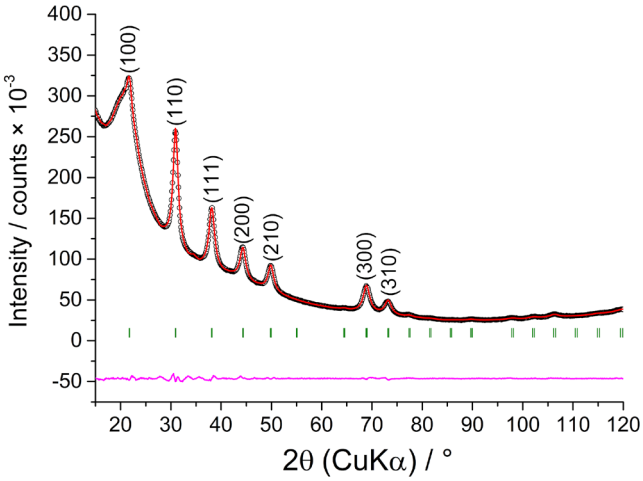

Figure 3. Rietveld refinement of the XRD pattern of the NaB_5C-related sodium carbaboride powder recovered after synthesis in molten sodium iodide: experimental pattern (dotted black), calculated pattern (red) and difference curve (purple). The green vertical bars correspond to the Bragg peak positions according to the NaB_5C structure. The broad bump between 15 and 30° is due to beam scattering by the protective PMMA plastic dome used to maintain the powder under protective argon atmosphere.

The composition of the material was confirmed by Energy dispersive X-ray spectroscopy (EDS), and X-ray photoelectron spectroscopy (XPS). Both techniques yield consistent molar Na/B ratios of 0.15 and 0.17, respectively (**Table S2**). These values confirm the sodium sub-stoichiometry inferred by XRD compared to the ideal stoichiometry NaB_5C. The absence of any band characteristic of graphitic ordering on the Raman spectrum (**Figure S2**) suggests that the sample is exempt of layered carbonaceous by-products and of amorphous carbon, which usually exhibits a slight portion of staked graphitic layers, thus giving rise to a Raman signature. The presence of methanol at the surface of the nanocrystals was confirmed by ^1H solid-state nuclear magnetic resonance (**Figure S3**), showing two peaks characteristic of methanol. The detectable amount of methanol is related to the high specific surface measured by nitrogen sorption around 300 $m^2\ g^{-1}$ according to the BET method. This high surface area

also results in surface carbonaceous contamination during analysis (**Table S2**), which precludes any precise estimation of the carbon content within the nanocrystals by XPS or electron energy loss spectroscopy, at the opposite of the bulk NaB_5C.[16]

The surface states were then further probed by XPS (**Figure S4**). According to the deconvolution of C 1s spectrum, four carbon chemical states were detected. The lowest binding energy peak at 283.06 eV is assigned to C-B bonds.[45] C-O bonds are also detected at 286.80 eV. They could arise from contamination and/or surface reactivity with methanol. The peaks at 284.81 eV and 289.04 eV come from adventitious carbon contamination.[45] The B 1s spectrum was deconvoluted into three peaks. The component at 187.02 eV corresponds to B-B bond.[45] The peak at 188.13 eV is assigned to B-C bonds.[45] Its relatively large FWHM indicates a distribution of boron chemical states round the B-C bonding boron, which could be explained by the various environments of boron atoms in the octahedra, with B atoms that can be linked to e.g. 3 B and 1 C, or 2 B and 2 C. The peak at 192.68 eV is characteristic of oxidized boron which could be ascribed to the high reactivity of the sample when exposed to air, during transfer to the XPS analysis chamber. This high reactivity, also observed by the pyrophoric nature of the dried samples when exposed a few seconds to air, was not reported for bulk sodium carbaboride[15,16] and is probably related to the small particle size and the very high surface-to-volume ratio. Despite surface oxidation and methanol adsorption, the particles are remarkably sodium borocarbide single nanocrystals. The consistency between the particle (TEM) and crystallite (XRD) sizes shows that oxidation impacts only the near surface of the nanocrystals when the samples are exposed only shortly to air.

The sub-stoichiometry of sodium we observe and the related carbon over-stoichiometry we propose for the sodium carbaboride nanocrystals are not in agreement with the ideal NaB_5C composition. Besides, addressing the validity of the electron counting rule in octahedra-based boron-rich compounds has been difficult to perform experimentally until now because of the

absence of a local probe for investigating the boron/carbon local environment. For these reasons, we have embarked on assessing the composition of the octahedra within sodium borocarbide nanocrystals by using ^{11}B solid-state NMR.

The ^{11}B solid-state NMR spectrum of NaB_5C shows at least three broad signals centered around 15, 2 and -8 ppm (**Figure 4**). No NMR study of AB_5C carbaborides has been reported and the case of boron carbides shows the complexity of assessing the structure of B and C-based solids with ^{11}B NMR.[46,47] For further assignment of the ^{11}B NMR signals, the spectrum was compared to spectra calculated by DFT based on several structural models (**Figure 5**). These models have been specifically designed in order to assess the composition of the octahedral units $B_{6-x}C_x$ and the ordering between these units (details for the construction of these models are given in the experimental section). The first model named **1Crandom222** accounts for the NaB_5C composition and consists in a 2x2x2 supercell with full Na occupancy with closed shell B_5C octahedra where the carbon atom is at a random position in all octahedra. The second model named **0C-2Crandom222** also accounts for the NaB_5C composition in a 2x2x2 supercell with full Na occupancy and built on octahedra, but with six of them being B_5C while the last two are one B_6 and one B_4C_2 octahedron, respectively. This model enables assessing deviation from the electron counting rule, as B_6 octahedra in the presence of Na cannot exhibit a 20-electrons closed shell. The third model named **1Crandom333** again accounts for the NaB_5C composition. It is equivalent to the model **1Crandom222**, but extended through a 3x3x3 supercell, with full Na occupancy and closed shell B_5C clusters where the carbon atom is randomly positioned. The fourth and fifth models account for the sodium sub-stoichiometry and carbon over-stoichiometries described above, by considering B_5C and B_4C_2 octahedra together. Each B_4C_2 unit is surrounded by a Na vacancy to ensure a closed shell octahedron. The fourth and fifth models are named **1Na-1C-2Crandom222** and **3Na-1C-2Crandom333**, respectively. They correspond to 2x2x2 and 3x3x3 supercells, respectively.

1Na-1C-2Crandom222 bears seven B_5C octahedra and one B_4C_2 octahedron next to one Na vacancy. **3Na-1C-2Crandom333** encompasses 24 B_5C octahedra and 3 B_4C_2 octahedron next to 3 Na vacancies. The atomic coordinates for the five structures were first DFT-relaxed before calculation of the NMR parameters through the gauge including projector augmented wave method. For comparison, NMR parameters were also calculated on a **single cell** (**Figure 4**), corresponding to a NaB_5C composition that would be equivalent to a supercell with full Na occupancy and closed shell B_5C octahedra where the carbon atom is at the same relative position in all octahedra. The results of these calculations are given in **Figure 4** and **Tables S3-S8**. The calculated NMR signals were then compared to the experimental ^{11}B NMR spectrum (**Figure 4**). First, the discrepancy between the experimental spectrum and the one calculated for the **single cell** model shows that carbon atoms are not located in the same relative position in each octahedron. Second and overall, a slightly better accuracy seems to be reached for model **3-Na-1C-2Crandom333**, which provides especially the best match of peak positions with the experimental spectrum. It should be noticed that the calculated parameters are not able to reproduce very accurately the experimental spectrum but since ^{11}B calculated quadruplar coupling constants are relatively small while boron atoms are close in space, the spectrum shape is probably dominated by dipolar couplings, which were not taken into account by the calculation. To illustrate this, broadened gaussian shapes were used for all models keeping calculated chemical shifts. The corresponding calculated spectra are presented **Figure S5**. As expected, the global agreement is more satisfactory.

In order to further confirm the presence of sodium vacancies and assess the existence of B_4C_2 units, the ^{23}Na MAS spectrum of NaB_5C was recorded. It shows a large signal centered around -6 ppm (**Figure S6**). This broadness could be either due to strong second-order quadrupolar effects or to a distribution of signals. To get clues on this question, the DFT calculated ^{23}Na spectra on the structural models previously described were compared to the

experimental one (**Figure S6**). The calculated parameters are summarized in **Tables S9-S10**. It appears that second-order quadrupolar effects are relatively small with quadrupolar coupling constants calculated between 230 and 1140 kHz. Consequently, the width of the experimental line can only be reproduced with a distribution of chemical shift values as observed in random models. The agreement with the experimental spectrum could probably be improved with larger models that would possibly allow a larger distribution but this would render NMR calculations too difficult with the current calculators. It can nonetheless be noticed that the highest averaged quadrupolar coupling constant in absolute value (> 700 kHz), which favors the line broadening, is observed in **0C-2Crandom222**, **1Na-1C-2Crandom222** and **3Na-1C-2Crandom333** models. This strongly suggests the presence of B_4C_2 octahedral clusters, in agreement with ^{11}B NMR. When combining ^{11}B and ^{23}Na results, the presence of B_5C and B_4C_2 octahedral clusters with Na vacancies around the latter gives the best agreement between experimental and theoretical data.

Overall, our results support a view where the as-synthesized sodium borocarbide nanocrystals encompass B_5C and B_4C_2 octahedral clusters. The former are surrounded by occupied Na sites, where Na provides one electron to yield formerly B_5C^- clusters, so that the solid obeys the stoichiometry NaB_5C in the short range. The environment of B_4C_2 octahedra is different as it contains Na vacancies, yielding the stoichiometry B_4C_2 at the short range. Both B_5C^- and B_4C_2 units meet the electron counting of 20 electrons for electronic stabilization. To our knowledge, B_4C_2 octahedral units or clusters have not been reported in inorganic solids, probably because of large strains to which they would be subjected. Their possible distortion will be studied in further work. Interestingly, the existence of B_4C_2 units has been previously suggested by Ivanovskii and Okatov who used DFT calculations to evaluate the electronic structure of NaB_5C and of an hypothetical cation-empty framework built only on B_4C_2 clusters.[48] These calculations suggest that such clusters associated to cation vacancies may

occur in NaB_5C-based structures, in agreement with our experimental results. However, it is intriguing to note that while B_4C_2 octahedral units have not been detected in bulk compounds, our results suggest that they might occur in nanocrystals. This could be related to the ability of nanocrystals to accommodate larger strains, and then to isolate such distorted structures, which are certainly metastable.

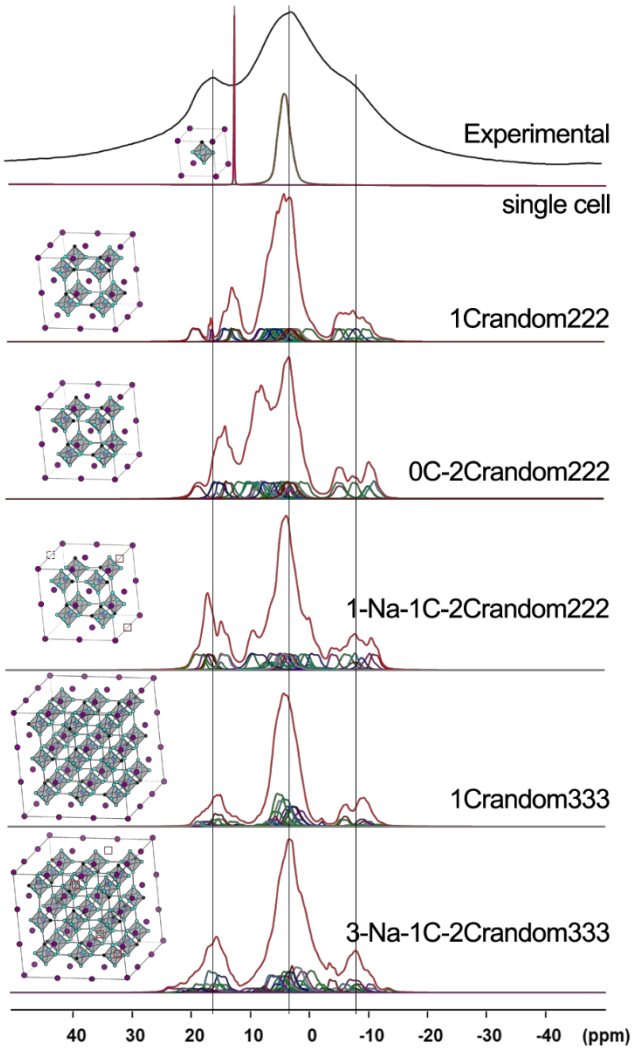

Figure 4. ^{11}B experimental solid-state NMR spectrum of NaB_5C-related sodium carbaboride powder and calculated spectra for the different structural models, detailed in Figure 5. The single cell spectrum is calculated from the reported structure of NaB_5C, where the carbon atom in B_5C octahedra is always at the same position (equivalent of a 2x2x2 or a 3x3x3 supercell with iso-located carbon atoms in each octahedral cluster). The three vertical lines are guides to the eye for the position of the three main features observed in the experimental spectrum.

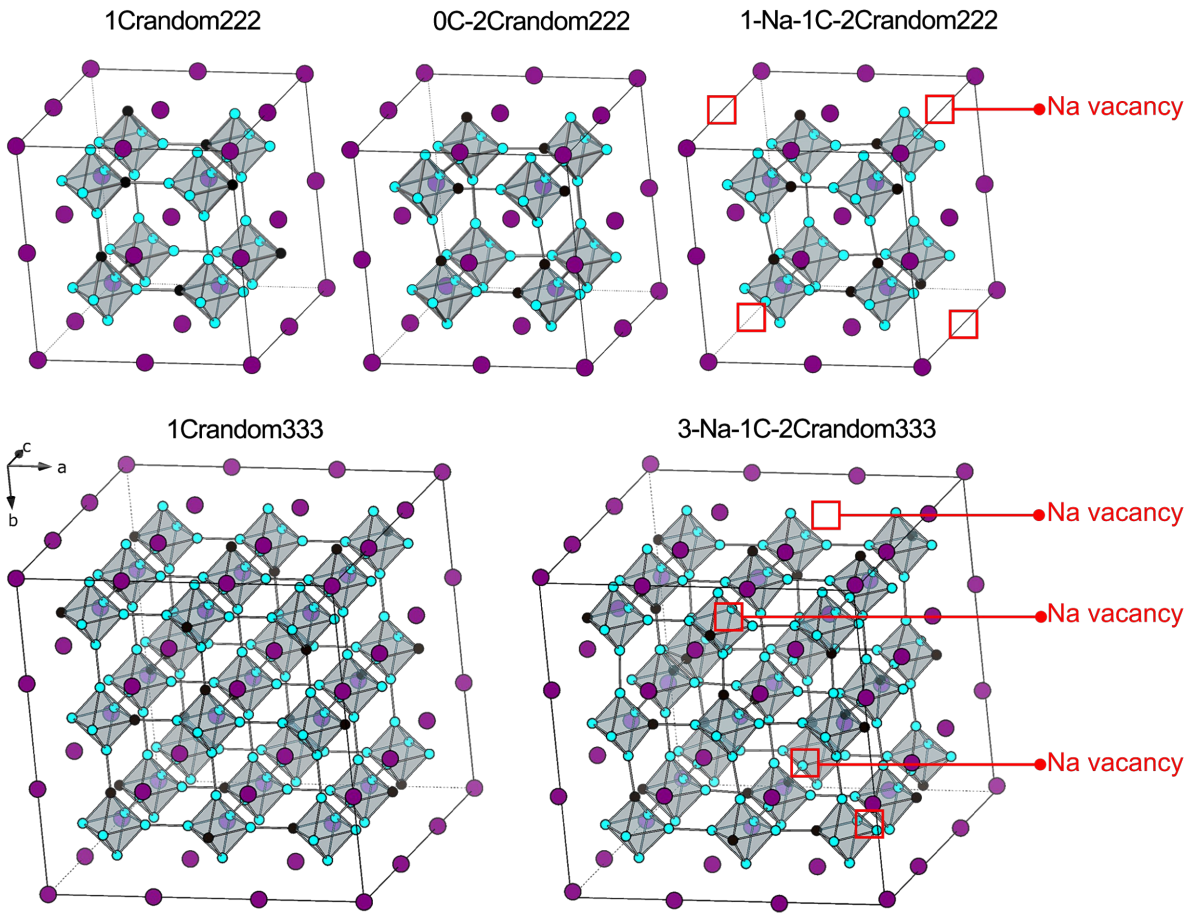

Figure 5. Structural models used to calculate the ^{11}B NMR spectra of sodium carbaborides. Boron, carbon and sodium atoms are in blue, black and purple, respectively. The octahedral clusters are represented in light grey. Sodium vacancies are represented with a red square.

High temperature transformation

The atom-scale mixture of boron and carbon in sodium carbaboride and the volatility of sodium might result in boron carbides upon thermal decomposition. Boron carbide, commonly known as black diamond, is an attractive material for its excelling hardness.[49] Rhombohedral boron carbides (**Figure 6** and **Movie S2**) exist as solid solutions usually presented in either its carbon-poor or its carbon-rich ideal stoichiometries: $B_{13}C_2$ (carbon content = 13 at.%) or B_4C (carbon content = 20 at.%), respectively. However, its solubility range further extends from 9.2 at.% to

21.6 at.% in carbon.[50] In its ideal stoichiometry, NaB_5C contains a C/(B+C) ratio of 0.17 at., while the refined formula of $Na_{0.816}B_{4.816}C_{1.184}$ corresponds to a ratio of 0.20 at., both within the solid solubility range for rhombohedral boron carbides. Such a broad coexistence between boron and carbon arises from the crystal structure of boron carbide, shown in **Figure 6**. Boron forms typical icosahedral clusters (B_{12}), bonded to one another by both direct covalent linkage between the polar position (B_p) and also through a 3 atoms covalent chain connecting equatorial (B_e) boron atoms. Both icosahedral positions and the three-atoms chains are susceptible of carbon substitution: B_{12}, $B_{11}C$, $B_{10}C_2$, and B_9C_3 icosahedra and CCC, CBC, CCB, CBB, BCB, and BBB chains have been suggested in the literature.[51,52]

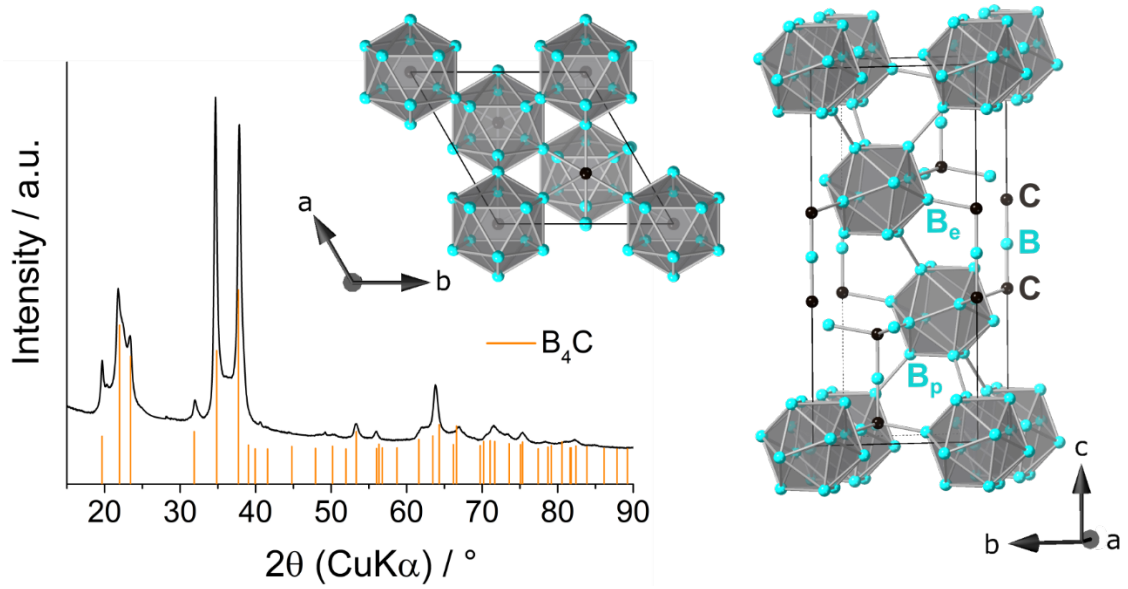

Figure 6. Powder XRD pattern of the powder obtained after calcination of sodium carbaboride nanocrystals. The reference pattern corresponds to rhombohedral B_4C-type boron carbide. Two different views of a corresponding ideal crystal structure are displayed.

We have then evaluated the thermal behavior of the molten salt-derived sodium carbaboride nanocrystals by calcining the powders under argon flow at 1200 °C. Upon heat treatment, the solid is thoroughly washed and analyzed. The X-ray diffraction pattern of the product is consistent with the expected one for boron carbide (**Figure 6**). TEM images of the resulting powder show well faceted nanoparticles of average edge size 9.9 nm according to a

lognormal fit of the edge length distribution of 100 nanoparticles (**Figure 7A**). High resolution TEM (**Figure 7B**) shows lattice fringes with distances characteristic of rhombohedral boron carbide crystal planes. As mentioned before, the complex covalent network of boron carbide yields high Vickers hardness values above the superhardness threshold (40 GPa). Further investigation of the impact of nanostructuration on the properties of boron carbide are underway.

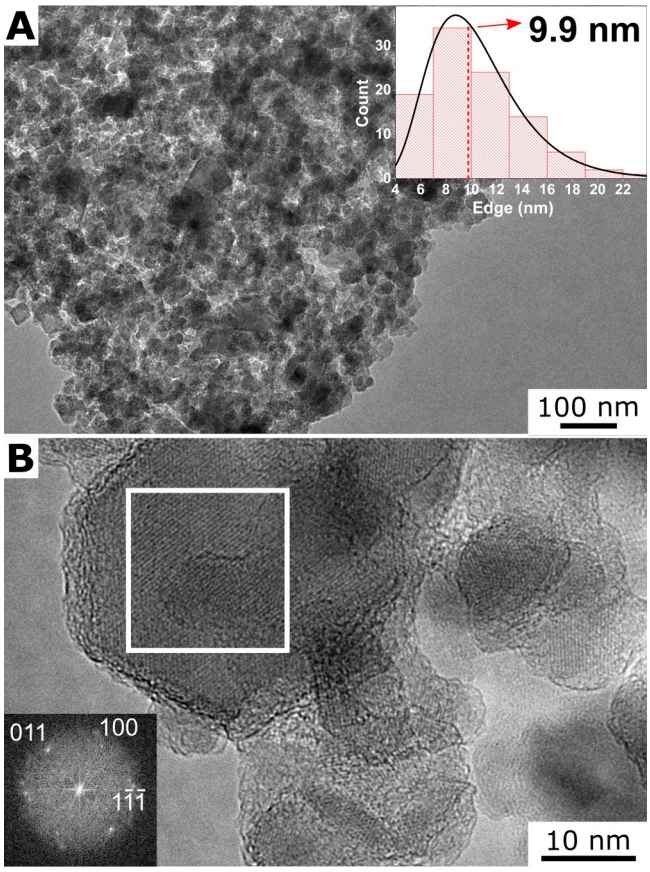

Figure 7. (A) TEM and (B) HRTEM images of boron carbide nanocrystals obtained by the decomposition of molten salt-derived sodium carbaboride nanocrystals. The inset in A shows the size distribution fitted with a lognormal function. The inset in B is a Fast Fourier Transform of the region marked with a white square. The reflexions are indexed along the rhombohedral boron carbide structure.

Conclusion

In conclusion, by using liquid-phase synthesis in molten salts, we have designed sodium carbaboride nanocrystals. These nanocrystals deviate from the ideal stoichiometry NaB_5C that

was reported up to now for the bulk compound. They show sodium vacancies which seem to be compensated by carbon over-stoichiometry in the octahedral units. As the model we propose is built on full octahedral units, the nanocrystals still obey the electron counting rule for full stabilization of an octahedral framework, but besides B_5C units, they also encompass B_4C_2 octahedral units, which to our knowledge have not been reported before in bulk inorganic compounds. This emerging diversity in octahedral structural building units in boron-based nano-objects might have a significant impact on the electronic and ionic conduction properties of these nanocrystals. Further study of the local structure around these units is then needed and will be addressed in a further work. More generally, widening the scope of covalent building blocks in boron-rich nano-objects compared to bulk compounds raises the question of the possible emergence of new boron-rich solids at the nanoscale, and then of possibly new properties, an issue that will deserve more efforts in the future. Finally, we provide the first evidence that such alkali-based nanocrystals can be used as efficient precursors to other boron-rich solids, especially boron carbides. These materials will require more in depth study but they already show that the reactivity of boron-rich nanoparticles may be used to target further complex covalent solids and materials.

Supporting information

The Supporting Information is available free of charge at https://pubs.acs.org/doi/xxx: Table S1 summarizing reported syntheses of sodium and potassium carbaborides, detailed XRD characterization in Figure S1, Raman, solid state ^{1}H NMR and X-ray photoelectron spectroscopic data in Figures S2, S3 and S4, respectively, XPS quantification in Table S2. details of ^{11}B and ^{23}Na solid state NMR calculations in Figures S5 and S6, respectively, with Tables S3 to S10.

Acknowledgements

SD and FI thank the French Ministry for Research (MESRI) for funding. SD, YLG and DP thank the CNRS for funding through the Energie cell. NMR spectroscopic calculations were performed using HPC resources from GENCI-IDRIS (Grant 097535). YS acknowledges funding from the China Scholarship Council. NMR and XPS facilities belong to Institut des Matériaux de Paris Centre. The authors thank Antoine Miche for XPS measurements.

References

(1) Albert, B.; Hillebrecht, H. Boron: Elementary Challenge for Experimenters and Theoreticians. *Angew. Chem. Int. Ed.* **2009**, *48*, 8640–8668. https://doi.org/10.1002/anie.200903246.

(2) Akopov, G.; Yeung, M. T.; Kaner, R. B. Rediscovering the Crystal Chemistry of Borides. *Adv. Mater.* **2017**, 1604506. https://doi.org/10.1002/adma.201604506.

(3) Mattox, T. M.; Agrawal, A.; Milliron, D. J. Low Temperature Synthesis and Surface Plasmon Resonance of Colloidal Lanthanum Hexaboride (LaB_6) Nanocrystals. *Chem. Mater.* **2015**, *27*, 6620–6624. https://doi.org/10.1021/acs.chemmater.5b02297.

(4) Li, L.; Sun, K.; Kurdak, C.; Allen, J. W. Emergent Mystery in the Kondo Insulator Samarium Hexaboride. *Nat. Rev. Phys.* **2020**, *2*, 463–479. https://doi.org/10.1038/s42254-020-0210-8.

(5) Longuet-Higgins, H. C.; Roberts, M. de V. The Electronic Structure of the Borides MB_6. *Proc. R. Soc. A Math. Phys. Eng. Sci.* **1954**, *224*, 336–347. https://doi.org/10.1098/rspa.1954.0162.

(6) Schmitt, K.; Stu, C.; Ripplinger, H.; Albert, B. Crystal and Electronic Structure of BaB_6 in Comparison with CaB_6 and Molecular $[B_6H_6]^{2-}$. *Solid State Sci.* **2001**, *3*, 321–327. https://doi.org/10.1016/S1293-2558(00)01091-8.

(7) Wade, K. The Structural Significance of the Number of Skeletal Bonding Electron-Pairs in Carboranes, the Higher Boranes and Borane Anions, and Various Transition-Metal Carbonyl Cluster Compounds. *J. Chem. Soc. D Chem. Commun.* **1971**, 15, 792–793. https://doi.org/10.1039/C29710000792.

(8) Mingos, D. M. P. A General Theory for Cluster and Ring Compounds of the Main Group and Transition Elements. *Nat. Phys. Sci.* **1972**, *236*, 99–102. https://doi.org/10.1038/physci236099a0.

(9) Jemmis, E. D.; Balakrishnarajan, M. M.; Pancharatna, P. D. A Unifying Electron-Counting Rule for Macropolyhedral Boranes, Metallaboranes, and Metallocenes. *J. Am. Chem. Soc.* **2001**, *123*, 4313–4323. https://doi.org/10.1021/ja003233z.

(10) Zintl, E. Intermetallische Verbindungen. *Angew. Chem.* **1939**, *52*, 1–6. https://doi.org/10.1002/ange.19390520102.

(11) Schäfer, H.; Eisenmann, B.; Müller, W. Zintl Phases: Transitions between Metallic and Ionic Bonding. *Angew. Chem. Int. Ed.* **1973**, *12*, 694–712. https://doi.org/https://doi.org/10.1002/anie.197306941.

(12) Mair, G.; von Schnering, H. G.; Wörle, M.; Nesper, R. Dilithium Hexaboride, Li2B6. *Zeitschrift für Anorg. und Allg. Chemie* **1999**, *625*, 1207–1211. https://doi.org/10.1002/(SICI)1521-3749(199907)625:7<1207::AID-ZAAC1207>3.0.CO;2-9.

(13) Naslain, R.; Etourneau, J. L'hexaborure de Potassium. *C. R. Acad. Sc.* **1966**, *263*, 484.

(14) Ammar, A.; Ménétrier, M.; Villesuzanne, A.; Matar, S.; Chevalier, B.; Etourneau, J.; Villeneuve, G.; Rodríguez-Carvajal, J.; Koo, H. J.; Smirnov, A. I.; Whangbo, M. H. Investigation of the Electronic and Structural Properties of Potassium Hexaboride, KB_6, by Transport, Magnetic Susceptibility, EPR, and NMR Measurements, Temperature-Dependent Crystal Structure Determination, and Electronic Band Structure Calculations. *Inorg. Chem.* **2004**, *43*, 4974–4987. https://doi.org/10.1021/ic049444c.

(15) Albert, B.; Schmitt, K. NaB_5C: Carbon Insertion into a Three-Dimensional Framework of Boron Octahedra Leads to Electron-Precise Cubic Carbaborides. *Chem. Commun.* **1998**, *21*, 2373–2374. https://doi.org/10.1039/a806994h.

(16) Albert, B.; Schmitt, K. New Boron-Rich Materials: Cubic Carbaborides of Sodium and Potassium. *Chem. Mater.* **1999**, *11*, 3406–3409. https://doi.org/10.1021/cm991130d.

(17) Soriano, R. B.; Arachchige, I. U.; Malliakas, C. D.; Wu, J.; Kanatzidis, M. G. Nanoscale Stabilization of New Phases in the $PbTe$-Sb_2Te_3 System: $Pb_mSb_{2n}Te_{m+3n}$ Nanocrystals. *J. Am. Chem. Soc.* **2013**, *135*, 768–774. https://doi.org/10.1021/ja309626q.

(18) Baitinger, M.; Böhme, B.; Ormeci, A.; Grin, Y. Solid State Chemistry of Clathrate Phases: Crystal Structure, Chemical Bonding and Preparation Routes. In *The Physics and Chemistry of Inorganic Clathrates*; Nolas, G. S., Ed.; Springer Science & Business Media: Dordrecht, 2014; p 332. https://doi.org/10.1007/978-94-017-9127-4.

(19) Thévenot, F. Boron Carbide-A Comprehensive Review. *J. Eur. Ceram. Soc.* **1990**, *6*, 205–225. https://doi.org/10.1016/0955-2219(90)90048-K.

(20) Liu, J.; Wen, S.; Hou, Y.; Zuo, F.; Beran, G. J. O.; Feng, P. Boron Carbides as Efficient, Metal-Free, Visible-Light-Responsive Photocatalysts. *Angew. Chem. Int. Ed.* **2013**, *52*, 3241–3245. https://doi.org/10.1002/anie.201209363.

(21) Morito, H.; Anzai, J.; Kimura, T.; Yamane, H. Synthesis of NaB_5C Bulk Ceramics by Reaction Sintering. *Solid State Sci.* **2015**, *47*, 39–42.

https://doi.org/10.1016/j.solidstatesciences.2015.03.013.

(22) Morito, H.; Kimura, T.; Yamane, H. NaB_5C–B_5/C Composite Ceramics Prepared by Reaction Sintering in Na Vapor. *J. Am. Ceram. Soc.* **2016**, *99*, 2422–2427. https://doi.org/10.1111/jace.14204.

(23) Carenco, S.; Portehault, D.; Boissière, C.; Mézailles, N.; Sanchez, C. Nanoscaled Metal Borides and Phosphides: Recent Developments and Perspectives. *Chem. Rev.* **2013**, *113*, 7981–8065. https://doi.org/10.1021/cr400020d.

(24) Portehault, D.; Delacroix, S.; Gouget, G.; Grosjean, R.; Chan-Chang, T.-H.-C. Beyond the Compositional Threshold of Nanoparticle-Based Materials. *Acc. Chem. Res.* **2018**, *51*, 930–939. https://doi.org/10.1021/acs.accounts.7b00429.

(25) Portehault, D.; Devi, S.; Beaunier, P.; Gervais, C.; Giordano, C.; Sanchez, C.; Antonietti, M. A General Solution Route toward Metal Boride Nanocrystals. *Angew. Chem. Int. Ed.* **2011**, *50*, 3262–3265. https://doi.org/10.1002/anie.201006810.

(26) Gouget, G.; Beaunier, P.; Portehault, D.; Sanchez, C. New Route toward Nanosized Crystalline Metal Borides with Tunable Stoichiometry and Variable Morphologies. *Faraday Discuss.* **2016**, *191*, 511–525. https://doi.org/10.1039/C6FD00053C

(27) Terlan, B.; Levin, A. A.; Börrnert, F.; Zeisner, J.; Kataev, V.; Schmidt, M.; Eychmueller, A. A Size-Dependent Analysis of the Structural, Surface, Colloidal, and Thermal Properties of $Ti_{1-x}B_2$ (x = 0.03-0.08) Nanoparticles. *Eur. J. Inorg. Chem.* **2016**, *2016*, 3460–3468. https://doi.org/10.1002/ejic.201600315.

(28) Terlan, B.; Levin, A.; Börrnert, F.; Simon, F.; Oschatz, M.; Schmidt, M.; Cardoso-Gil, R.; Lorenz, T.; Baburin, I.; Joswig, J.-O.; Eychmueller, A. Effect of Surface Properties on the Microstructure, Thermal and Colloidal Stability of VB_2 Nanoparticles. *Chem. Mater.* **2015**, *27*, 5106–5115. https://doi.org/10.1021/acs.chemmater.5b01856.

(29) Ma, J. L.; Li, N.; Zhang, Q.; Zhang, X. B.; Wang, J.; Li, K.; Hao, X. F.; Yan, J. M. Synthesis of Porous and Metallic CoB Nanosheets towards a Highly Efficient Electrocatalyst for Rechargeable Na-O_2 Batteries. *Energy Environ. Sci.* **2018**, *11*, 2833–2838. https://doi.org/10.1039/c8ee01472h.

(30) Yu, Y.; Wang, S.; Li, W.; Chen, Z. Low Temperature Synthesis of LaB_6 Nanoparticles by a Molten Salt Route. *Powder Technol.* **2018**, *323*, 203–207. https://doi.org/10.1016/j.powtec.2017.09.049.

(31) Yu, Y.; Wang, S.; Li, W.; Chen, H.; Chen, Z. Synthesis of Single-Crystalline Lanthanum Hexaboride Nanocubes by a Low Temperature Molten Salt Method. *Mater. Chem. Phys.* **2018**, *207*, 325–329. https://doi.org/10.1016/j.matchemphys.2017.12.081.

(32) Groome, C.; Roh, I.; Mattox, T. M.; Urban, J. J. Effects of Size and Structural Defects on the Vibrational Properties of Lanthanum Hexaboride Nanocrystals. *ACS Omega* **2017**, *2*, 2248–2254. https://doi.org/10.1021/acsomega.7b00263.

(33) Gouget, G.; Debecker, D. P.; Kim, A.; Olivieri, G.; Gallet, J.-J.; Bournel, F.; Thomas, C.; Ersen, O.; Moldovan, S.; Sanchez, C.; Carenco, S.; Portehault, D. *In Situ* Solid-Gas

Reactivity of Nanoscaled Metal Borides from Molten Salt Synthesis. *Inorg. Chem.* **2017**, *56*, 9225–9234. https://doi.org/10.1021/acs.inorgchem.7b01279.

(34) Delacroix, S.; Le Godec, Y.; Coelho-Diogo, C.; Gervais, C.; Génois, I.; Le Griel, P.; Portehault, D. Synthesis in Molten Salts and Characterization of $Li_6B_{18}(Li_2O)_x$ Nanoparticles. *Inorg. Chem.* **2020**, *18*, 2–7. https://doi.org/10.1021/acs.inorgchem.0c01694.

(35) Rodriguez-Carvajal, J. FullProf Suite; All the Programs Can Be Obtained from: Http://Www.Ill.Eu/Sites/Fullprof. Laboratoire Léon Brillouin, CEA: Saclay, France.

(36) Kresse, G.; Hafner, J. Ab Initio Molecular-Dynamics Simulation of the Liquid-Metal--Amorphous-Semiconductor Transition in Germanium. *Phys. Rev. B* **1994**, *49*, 14251–14269. https://doi.org/10.1103/PhysRevB.49.14251.

(37) Giannozzi, P.; Baroni, S.; Bonini, N.; Calandra, M.; Car, R.; Cavazzoni, C.; Ceresoli, D.; Chiarotti, G. L.; Cococcioni, M.; Dabo, I.; Dal Corso, A.; de Gironcoli, S.; Fabris, S.; Fratesi, G.; Gebauer, R.; Gerstmann, U.; Gougoussis, C.; Kokalj, A.; Lazzeri, M.; Martin-Samos, L.; Marzari, N.; Mauri, F.; Mazzarello, R.; Paolini, S.; Pasquarello, A.; Paulatto, L.; Sbraccia, C.; Scandolo, S.; Sclauzero, G.; Seitsonen, A. P.; Smogunov, A.; Umari, P.; Wentzcovitch, R. M. QUANTUM ESPRESSO: A Modular and Open-Source Software Project for Quantum Simulations of Materials. *J. Phys. Condens. Matter* **2009**, *21*, 395502. https://doi.org/10.1088/0953-8984/21/39/395502.

(38) Perdew, J. P.; Burke, K.; Ernzerhof, M. Generalized Gradient Approximation Made Simple. *Phys. Rev. Lett.* **1996**, *77*, 3865–3868. https://doi.org/10.1103/physrevlett.77.3865

(39) Troullier, N.; Martins, J. L. Efficient Pseudopotentials for Plane-Wave Calculations. *Phys. Rev. B* **1991**, *43*, 1993–2006. https://doi.org/10.1103/PhysRevB.43.1993

(40) Kleinman, L.; Bylander, D. Efficacious Form for Model Pseudopotentials. *Phys. Rev. Lett.* **1982**, *48*, 1425. https://doi.org/10.1103/PhysRevLett.48.1425

(41) Pickard, C.; Mauri, F. All-Electron Magnetic Response with Pseudopotentials: NMR Chemical Shifts. *Phys. Rev. B* **2001**, *63*, 245101. https://doi.org/10.1103/PhysRevB.63.245101

(42) Mayen, L.; Jensen, N. D.; Desbord, M.; Laurencin, D.; Gervais, C.; Bonhomme, C.; Smith, M. E.; Porcher, F.; Elkaim, E.; Charvillat, C.; Gras, P.; Rey, C.; Soulié, J.; Combes, C. Advances in the Synthesis and Structure of α-Canaphite: A Multitool and Multiscale Study. *CrystEngComm* **2020**, *22*, 3130–3143. https://doi.org/10.1039/D0CE00132E.

(43) Pyykkö, P. Year-2008 Nuclear Quadrupole Moments. *Mol. Phys.* **2008**, *106*, 1965–1974. https://doi.org/10.1080/00268970802018367

(44) Massiot, D.; Fayon, F.; Capron, M.; King, I.; Le Calvé, S.; Alonso, B.; Durand, J. O.; Bujoli, B.; Gan, Z.; Hoatson, G. Modelling One- and Two-Dimensional Solid-State NMR Spectra. *Magn. Reson. Chem.* **2002**, *40*, 70–76. https://doi.org/10.1002/mrc.984.

(45) Zhang, S.; Lu, W.; Wang, C.; Shen, Q.; Zhang, L. Stoichiometric Controlling of Boron

Carbide Thin Films by Using Boron-Carbon Dual-Targets. *Appl. Phys. Lett.* **2012**, *101*, 141602. https://doi.org/10.1063/1.4754628.

(46) Kirkpatrick, R. J.; Aselage, T.; Phillips, B. L.; Montez, B. ^{11}B and ^{13}C NMR Spectroscopy of Boron Carbides. *AIP Conf. Proc.* **1991**, 261–270. https://doi.org/10.1063/1.40836.

(47) Pallier, C.; Leyssale, J.-M.; Truflandier, L. A.; Bui, A. T.; Weisbecker, P.; Gervais, C.; Fischer, H. E.; Sirotti, F.; Teyssandier, F.; Chollon, G. Structure of an Amorphous Boron Carbide Film: An Experimental and Computational Approach. *Chem. Mater.* **2013**, *25*, 2618–2629. https://doi.org/10.1021/cm400847t.

(48) Ivanovskii, A. L.; Okatov, S. V. The Electronic Structure of the New Cubic Carbaboride NaB_5C as Compared to CaB_6 and "B_4C_2" by the Full-Potential LMTO Method. *Mendeleev Commun.* **2001**, *11*, 8–9. https://doi.org/10.1070/mc2001v011n01abeh001393.

(49) Domnich, V.; Gogotsi, Y.; Trenary, M.; Tanaka, T. Nanoindentation and Raman Spectroscopy Studies of Boron Carbide Single Crystals. *Appl. Phys. Lett.* **2002**, *81*, 3783–3785. https://doi.org/10.1063/1.1521580.

(50) Beauvy, M. Stoichiometric Limits of Carbon-Rich Boron Carbide Phases. *J. Less Common Met.* **1983**, *90*, 169–175. https://doi.org/https://doi.org/10.1016/0022-5088(83)90067-X.

(51) Domnich, V.; Reynaud, S.; Haber, R. a.; Chhowalla, M. Boron Carbide: Structure, Properties, and Stability under Stress. *J. Am. Ceram. Soc.* **2011**, *94*, 3605–3628. https://doi.org/10.1111/j.1551-2916.2011.04865.x.

(52) Rasim, K.; Ramlau, R.; Leithe-Jasper, A.; Mori, T.; Burkhardt, U.; Borrmann, H.; Schnelle, W.; Carbogno, C.; Scheffler, M.; Grin, Y. Local Atomic Arrangements and Band Structure of Boron Carbide. *Angew. Chem. Int. Ed.* **2018**, *57*, 6130–6135. https://doi.org/https://doi.org/10.1002/anie.201800804.

Table of content graphic

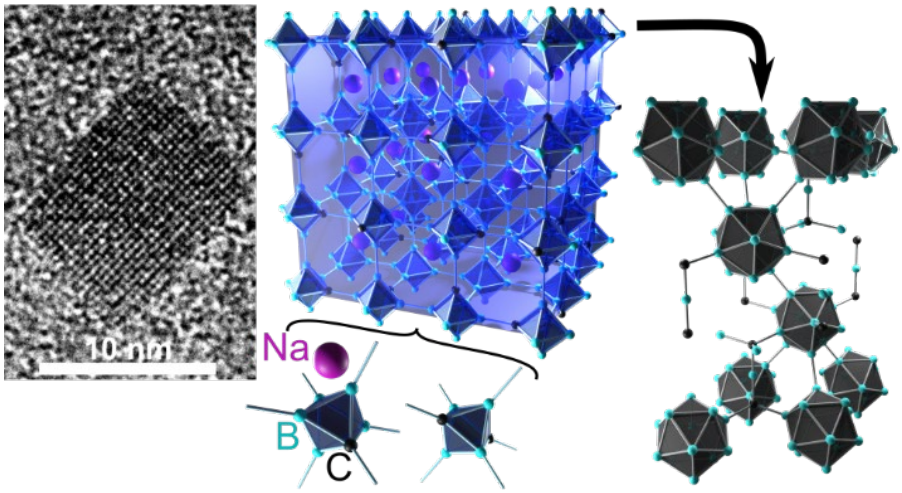

Table of content synopsis

Sodium borocarbide nanocrystals synthesized in molten salts provide the opportunity to explore for the first time the reactivity of these cluster-based solids. They also enable addressing the fundamental question about how electron counting rules in boron-rich solids apply in nanocrystals with stoichiometries that deviate from the previously known bulk cases. We show that these nanocrystals evolve towards boron carbide upon heating and that they fulfill electron counting rules by accommodating alternative cluster compositions.

Supporting information

Electron precise sodium carbaboride nanocrystals from molten salts: single sources to boron carbides

Simon Delacroix,[1,2] Fernando Igoa,[1,2] Yang Song,[1] Yann Le Godec,[2,*] Cristina Coelho-Diogo,[3] Christel Gervais,[1] Gwenaelle Rousse,[4] David Portehault[1,*]

[1] Sorbonne Université, CNRS, Collège de France, Laboratoire de Chimie de la Matière Condensée de Paris (CMCP), 4 place Jussieu, F-75005, Paris, France

[2] Sorbonne Université, CNRS, MNHN, IRD, Institut de Minéralogie, de Physique des Matériaux et de Cosmochimie (IMPMC), 4 place Jussieu, F-75005, Paris, France

[3] Sorbonne Université, CNRS, Institut des Matériaux de Paris Centre (IMPC), 4 place Jussieu, F-75005, Paris, France

[4] Collège de France, Sorbonne Université, Chimie du Solide et de l'Energie (CSE), 75231 Paris Cedex 05, France

*Corresponding authors:

david.portehault@sorbonne-universite.fr

yann.le_godec@sorbonne-universite.fr

Table S1. Synthesis conditions of alkali carbaborides NaB_5C and KB_5C reported in the literature. Numbered references are those of the main text.

Compound	Time (h)	Temperature (°C)	Precursors	Method
NaB_5C[15]	2	1050	Na, B, $C_{(gr)}$	Sealed vessel
NaB_5C[21,22]	24	900	Na, B, $C_{(am)}$	Na flux in sealed vessel
KB_5C[51]	16	1100	K, B, $C_{(gr)}$	Sealed vessel
NaB_5C (this work)	2	900	$NaBH_4$, polyethylene	Molten NaI in open vessel

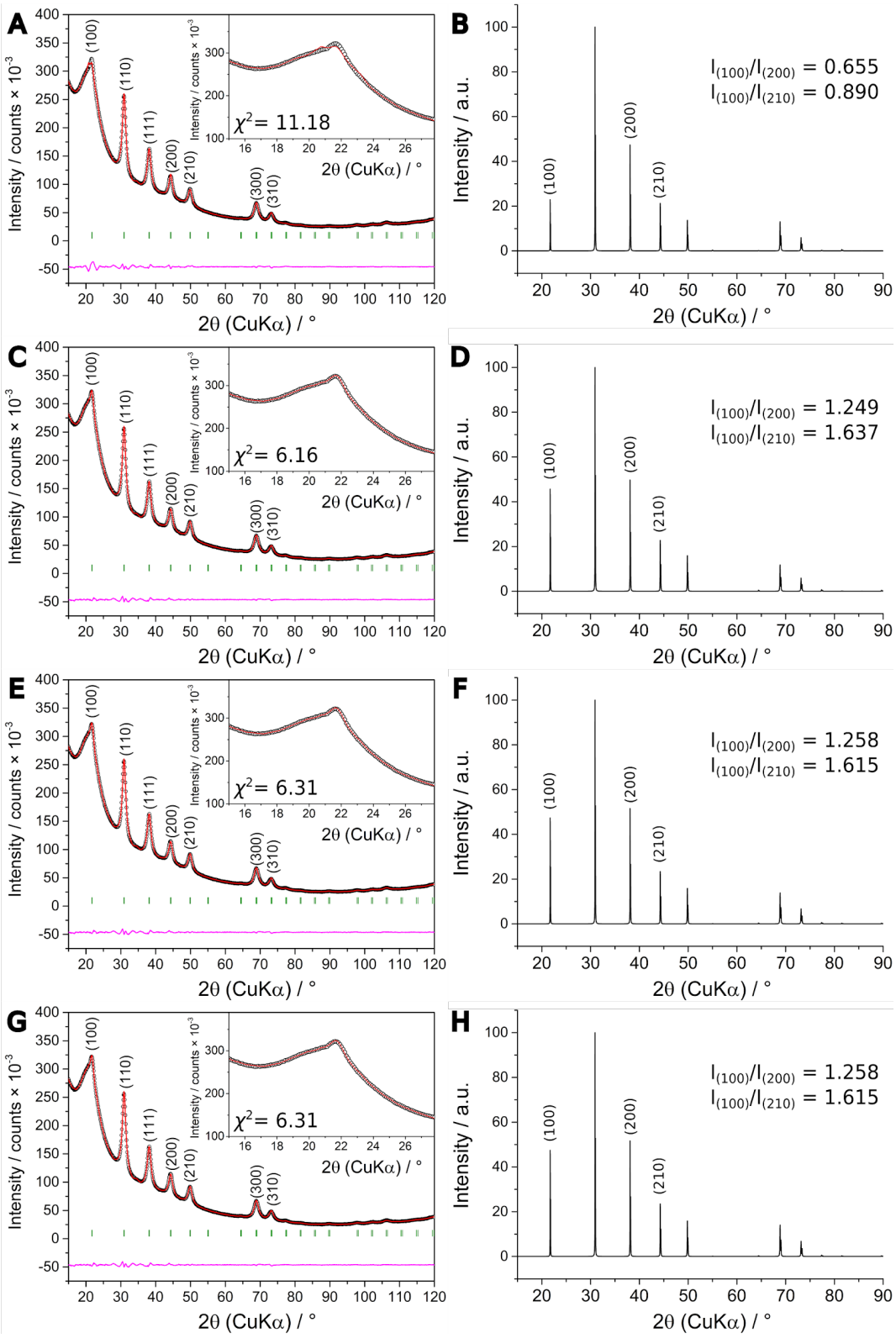

Figure S1. Consecutive Rietveld refinement of NaB_5C. (A) No occupation refinement. (B) Simulated XRD powder diffractogram from model considered in (A). (C) Model I, B to C ratio refinement. (D) Simulated XRD powder diffractogram from model considered in (C). (E) Model II, Na occupation refinement. (F) Simulated XRD powder diffractogram from model considered in (E). (G) Model III, occupancies refined restrained to the $Na_{1-x}B_{5-x}C_{1+x}$. formula. (H) Simulated XRD powder diffractogram from model considered in (G).

Table S2. Crystallographic data of sodium borocarbide obtained by refinement of the structure from the X-Ray powder diffraction data at room temperature, according to model III (Figure S1 G-H).

Space group	$Pm\bar{3}m$
***a, b, c* (Å)**	4.0878(2)
***α, β, γ* (°)**	90
Volume (Å^3)	68.3062(4)
R_{Bragg} (%)	0.66
R_{WP} (%)	5.41
χ^2	6.31

Atom	Wyckoff	*x*	*y*	*z*	B_{iso} (Å^2)	Occupation
Na1	1*a*	0	0.0000	0.0000	3.84(9)	0.816(2)
B1	6*f*	½	0.5000	0.8006(4)	2.93(5)	0.803(2)
C1	6*f*	½	0.5000	0.8006(4)	2.93(5)	0.197(2)

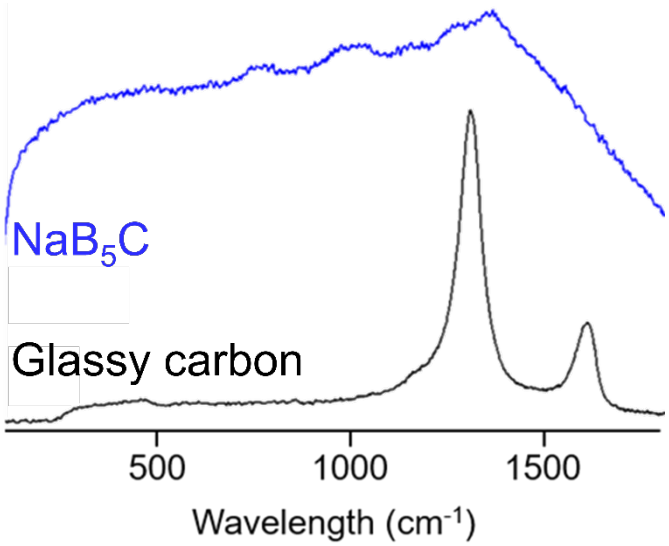

Figure S2. Raman spectra of sodium borocarbide nanocrystals (blue). The spectrum of glassy carbon is given as a reference (black), showing the two typical bands of disordered carbon with graphitic domains.

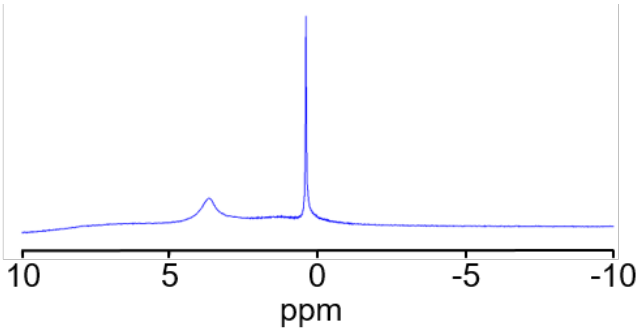

Figure S3. Solid state ^{1}H NMR spectrum of sodium borocarbide nanocrystals.

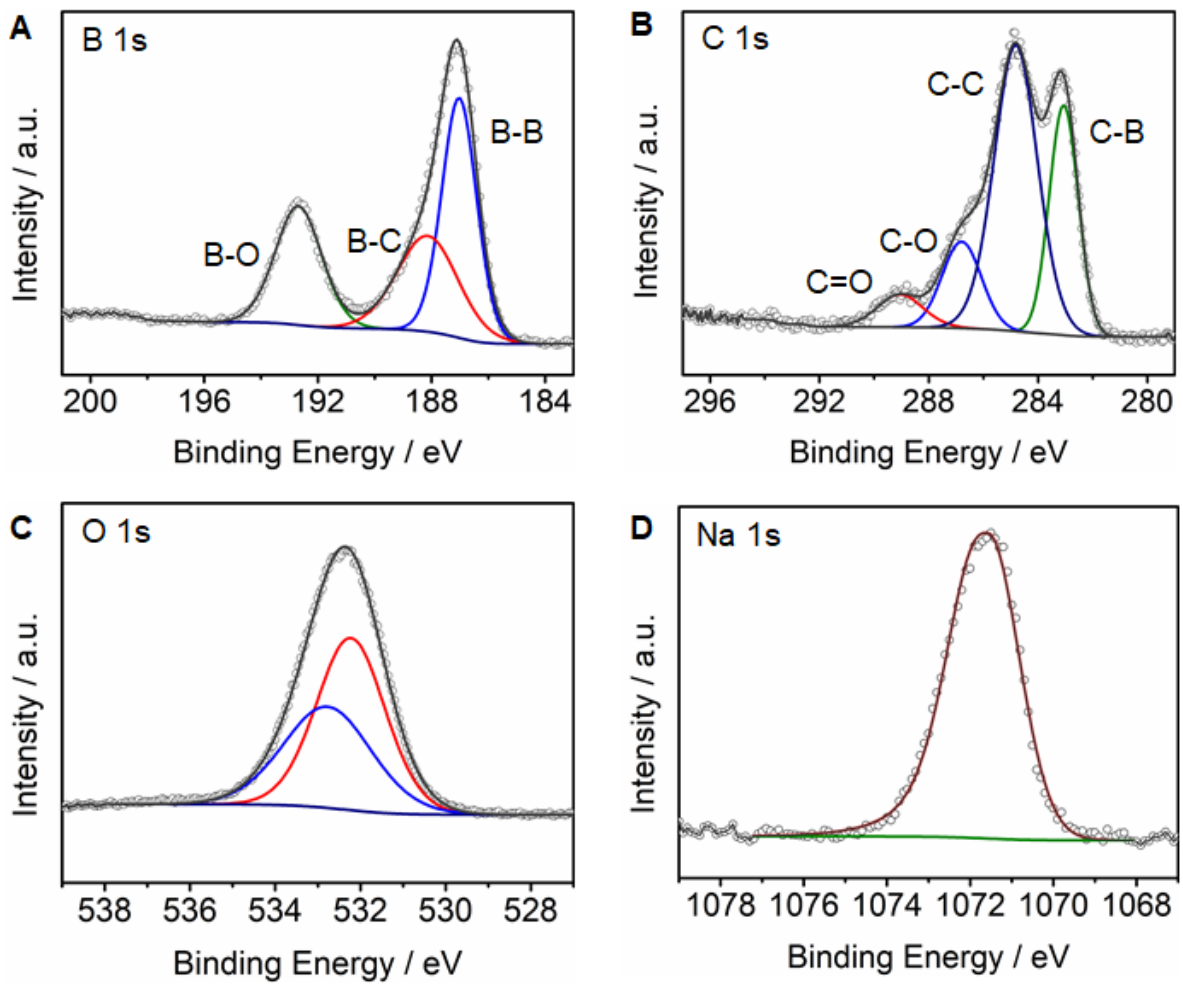

Figure S4. X ray photoelectron spectra of sodium carbaboride nanocrystals: (A) B 1s region, (B) C 1s region, (C) O 1s region, (D) Na 1s region

XPS data quantification

Composition quantification of the sample was done with the software Thermo Avantage©. This simplified calculation assumed that all elements are homogeneously distributed on depth. In order to yield a consistent approximation quantification, several factors were taken into account to normalize the peak area, including the sensitivity factor (SF), instrument transmission function (TXFN), and energy compensation factor (ECF). In this work, the SF was chosen with ALSCOF peak library, and the ECF was evaluated through the TPP-2M method, in order to calculate the inelastic mean free paths (IMFP). From the quantification results based on XPS data (**Table S1**), the overall B/C ratio is 3.2. This ratio accounts for contamination carbon and structural carbon. Because contamination cannot be avoided with the high surface area of the material, the carbon content within the nanocrystals cannot be evaluated exactly. A similar effect has been observed when evaluating the B/C ratio by STEM-EELS on a holey silica grid, which yielded a similar value.

Table S3. XPS quantification table.

Deconvoluted peaks		BE (eV)	Relative ratio (at.%)
B 1s	B-B	187.02	29
	B-C	188.13	20
	B-O	192.68	19
C 1s	C-B	283.06	6
	C-C	284.81	11
	C-O	286.80	3
	C=O	289.04	1
Na 1s	sodium salt	1071.57	11

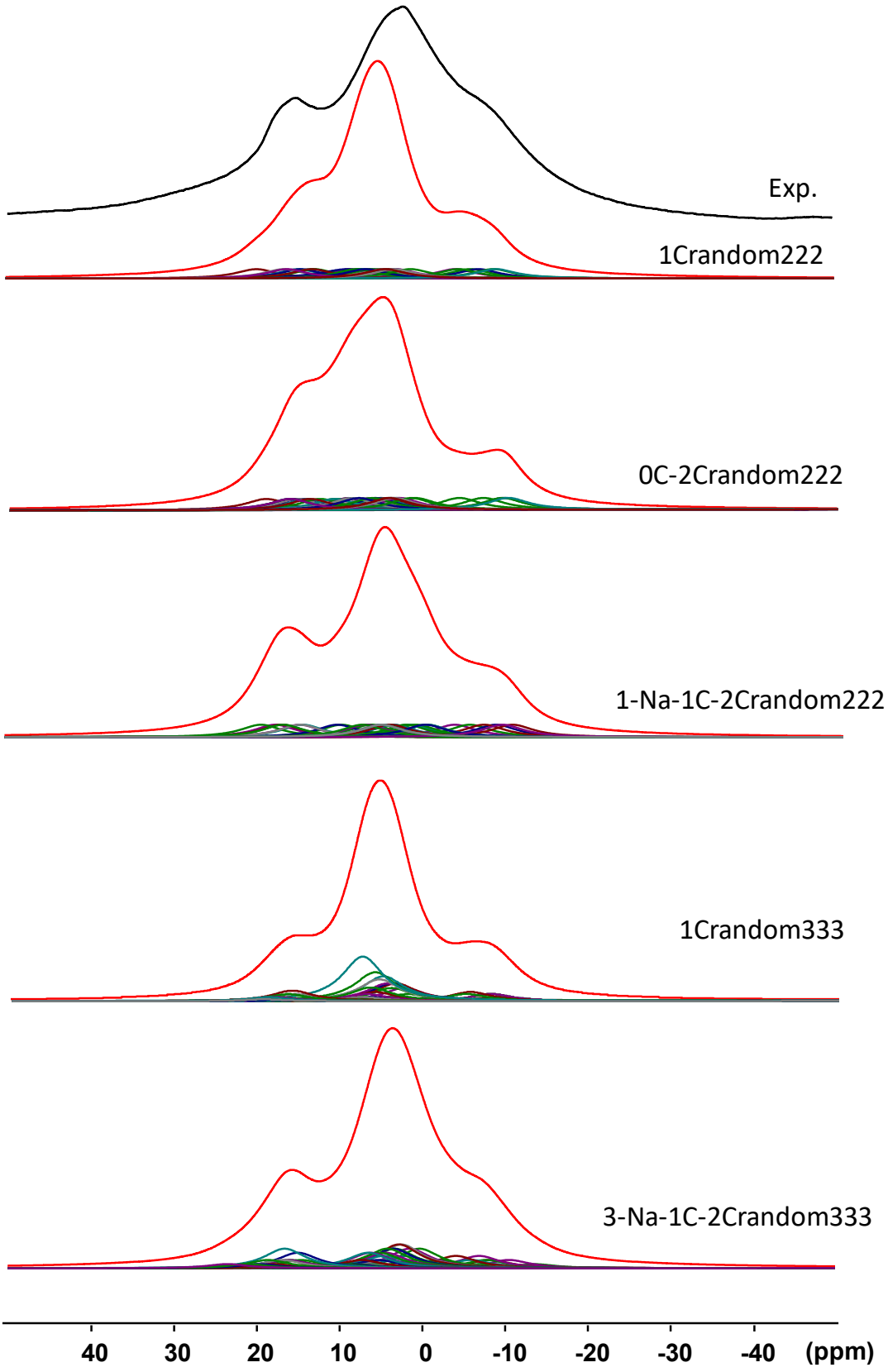

Figure S5. ^{11}B experimental solid-state NMR spectrum of NaB_5C-related sodium carbaboride powder and calculated spectra of the different models proposed replacing quadrupolar lineshapes by broadened Gaussian lines.

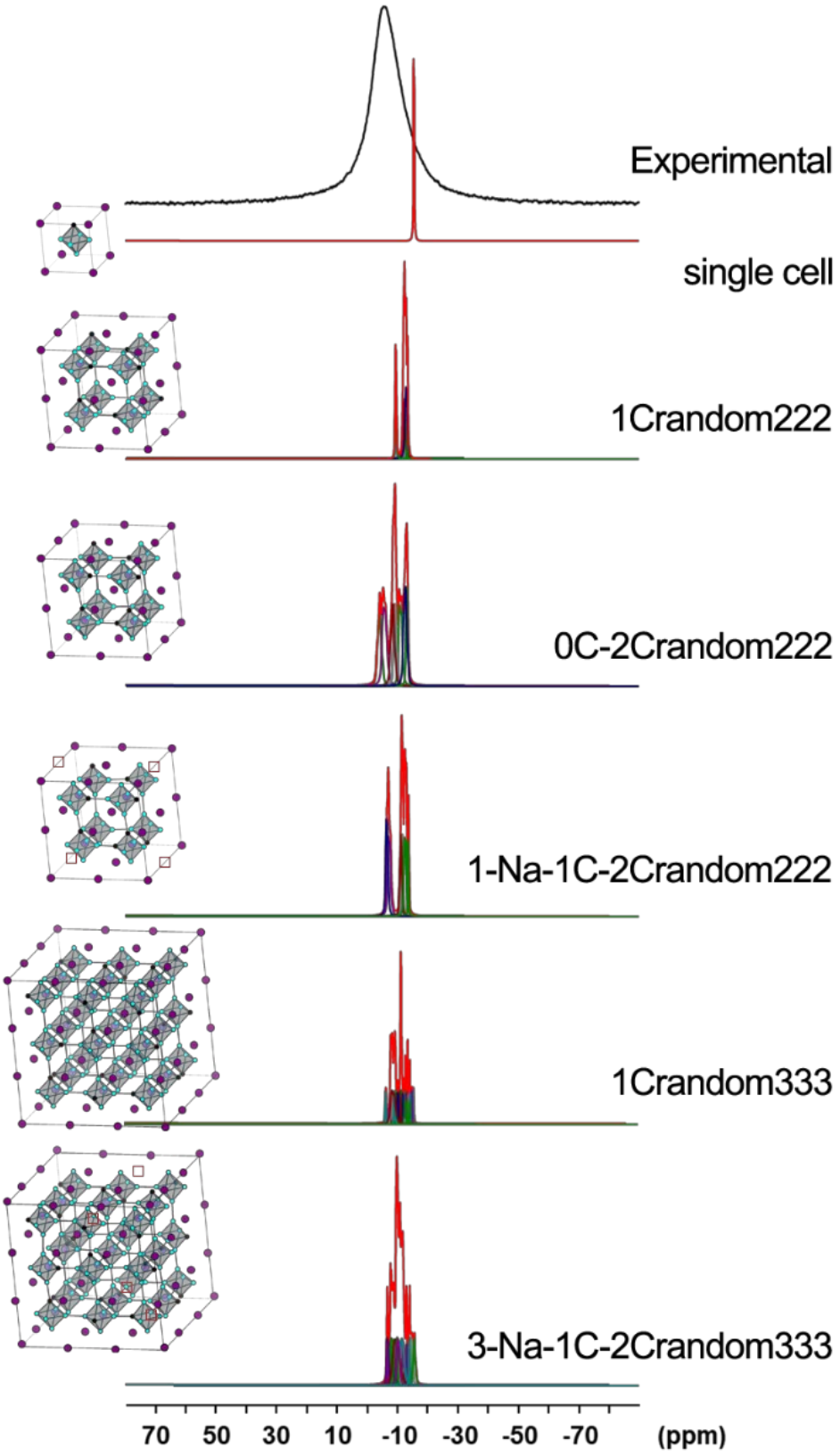

Figure S6. ^{23}Na experimental solid-state NMR spectrum of NaB_5C-related sodium carbaboride powder and calculated spectra for the different structural models, detailed in Figure 5 of the main text. The single cell spectrum is calculated from the reported structure of NaB_5C, where the carbon atom in B_5C octahedra is always at the same position (equivalent of a 2x2x2 or a 3x3x3 supercell with iso-located carbon atoms in each octahedral cluster).

Table S4. Crystallographic data of the **1Crandom222** model (occupancy is 1 for all atoms).

Space group	*P1*
***a, b, c* (Å)**	8.1848
***α, β, γ* (°)**	90

Atom	***x***	***y***	***z***
B1	0.41567923	0.74877276	0.25844785
B2	0.11362724	0.24805481	0.74825343
B3	0.26368005	0.25134904	0.89674660
B4	0.41658274	0.24992639	0.74843991
B5	0.25942187	0.40062633	0.74459778
B6	0.26092943	0.74950168	0.10896587
B7	0.11281897	0.74806665	0.25814057
B8	0.25828437	0.75327947	0.41201448
B9	0.74648637	0.89648115	0.74818651
B10	0.26151212	0.90080020	0.25746276
B11	0.73557069	0.39698255	0.24864831
B12	0.08813966	0.75690838	0.75084005
B13	0.24281487	0.60655958	0.74826239
B14	0.24464921	0.75307547	0.90213276
B15	0.39131434	0.75606960	0.74935149
B16	0.24528155	0.90977610	0.75137830
B17	0.73559335	0.24754956	0.09922501
B18	0.58056283	0.25031425	0.24876948
B19	0.26343755	0.24886892	0.59894115
B20	0.73530937	0.09820252	0.24864056
B21	0.75411426	0.24693577	0.59973514
B22	0.74637364	0.74752175	0.89673752
B23	0.74734867	0.59859051	0.74825689
B24	0.59668760	0.74905982	0.74534722
B25	0.74752725	0.74755350	0.59894985
B26	0.75341263	0.89525446	0.24881542
B27	0.90639577	0.74412637	0.25043144
B28	0.75678234	0.74685857	0.39790926
B29	0.75317487	0.59773290	0.24887044
B30	0.24266133	0.40997587	0.25233277
B31	0.75601922	0.74693980	0.09972925
B32	0.75725919	0.39547566	0.74863162
B33	0.90710186	0.24407293	0.74869764
B34	0.75398194	0.24695003	0.89757775
B35	0.75610093	0.09749135	0.74865222
B36	0.24265321	0.25541433	0.09919182
B37	0.08287637	0.25613927	0.24878567
B38	0.24169427	0.10608591	0.24935907
B39	0.24216631	0.25328213	0.39839974
B40	0.73584644	0.24751038	0.39792823
C1	0.61412814	0.74476389	0.25144510

C2	0.26184056	0.60725046	0.25973228
C3	0.37999548	0.25661684	0.24914952
C4	0.87688308	0.24954851	0.24866533
C5	0.88869223	0.75000417	0.74626745
C6	0.24373003	0.75554713	0.60863191
C7	0.61487804	0.24511733	0.74850685
C8	0.26041506	0.10739938	0.74662314
Na1	0.50656418	0.99108187	0.99842819
Na2	0.50694671	0.50350787	0.98721665
Na3	0.51311516	0.99687065	0.50005098
Na4	0.99485082	0.49786866	0.99262505
Na5	0.98944568	0.49208753	0.50412743
Na6	0.99424268	0.99814700	0.00469745
Na7	0.98910387	0.00293471	0.49235125
Na8	0.51329439	0.49711729	0.50969718

Table S5. Crystallographic data of the **0C-2Crandom222** model (occupancy is 1 for all atoms).

Space group	*P1*
***a, b, c* (Å)**	8.1848
***α, β, γ* (°)**	90

Atom	***x***	***y***	***z***
B1	0.41187720	0.74492394	0.25804653
B2	0.11242339	0.24650157	0.74852633
B3	0.26266035	0.25023722	0.89710000
B4	0.41525855	0.24882842	0.74857669
B5	0.26022834	0.39933435	0.74519320
B6	0.25926697	0.74849759	0.10835420
B7	0.11072882	0.74405678	0.25902902
B8	0.25876262	0.75216839	0.41302401
B9	0.74604843	0.89469193	0.74786253
B10	0.25963411	0.89961364	0.25781434
B11	0.73455604	0.40866331	0.24877533
B12	0.10125467	0.75649936	0.74866425
B13	0.25153598	0.60592194	0.74900965
B14	0.25225846	0.75221465	0.90136226
B15	0.39933484	0.75500569	0.74922154
B16	0.25348875	0.90815132	0.75201016
B17	0.73563074	0.25524922	0.09892092
B18	0.57954631	0.25819730	0.24902432
B19	0.26244276	0.24805321	0.59921549
B20	0.73498614	0.10575432	0.24871536
B21	0.75298097	0.24704045	0.60028063
B22	0.89791262	0.74826861	0.74502538
B23	0.74651755	0.74307858	0.89656238

B24	0.74700323	0.59538708	0.74790785
B25	0.59875509	0.74644401	0.74539334
B26	0.74640408	0.74316242	0.59851728
B27	0.75240000	0.89630730	0.24863227
B28	0.90173876	0.74440662	0.25084393
B29	0.74880229	0.74451871	0.39832105
B30	0.24195276	0.40917174	0.25252012
B31	0.74888364	0.74420197	0.09882141
B32	0.75263061	0.39405750	0.74868089
B33	0.90445158	0.24272258	0.74887980
B34	0.75274660	0.24703247	0.89728221
B35	0.75088949	0.09593671	0.74866500
B36	0.24236494	0.25446895	0.09943979
B37	0.08270611	0.25899943	0.24901975
B38	0.24064954	0.10577733	0.24979710
B39	0.24183531	0.25258676	0.39880808
B40	0.73592937	0.25515924	0.39861099
C1	0.61109246	0.74501095	0.25057126
C2	0.26054441	0.60535718	0.25969931
C3	0.37937360	0.25798695	0.24939557
C4	0.87708578	0.25889397	0.24886064
C5	0.75105060	0.60569771	0.24884313
C6	0.25265881	0.75424267	0.60934413
C7	0.61261275	0.24435873	0.74862069
C8	0.26161749	0.10633508	0.74695543
Na1	0.50638675	0.99007868	0.98670774
Na2	0.50188830	0.50434089	0.97105559
Na3	0.51212583	0.99581465	0.51104737
Na4	0.00077493	0.50111186	0.96905867
Na5	0.99553712	0.49582163	0.52725643
Na6	0.99249361	0.99083717	0.98519891
Na7	0.98755228	0.99500459	0.51145093
Na8	0.50772722	0.49781465	0.52547884

Table S6. Crystallographic data of the **1Crandom333** model (occupancy is 1 for all atoms).

Space group	*P1*
***a, b, c* (Å)**	12.2772
***α, β, γ* (°)**	90

Atom	***x***	***y***	***z***
B1	0.16437790	0.93206549	0.49240358
B2	0.40731945	0.83503852	0.16399885
B3	0.16001447	0.17206294	0.93624598
B4	0.94283528	0.15678575	0.83202604
B5	0.16338624	0.50157663	0.40889285
B6	0.16000271	0.26841789	0.82973985

B7	0.60354277	0.17997699	0.16064547
B8	0.50095545	0.16242808	0.40109484
B9	0.59872164	0.50527322	0.49514391
B10	0.50265886	0.50222367	0.59745662
B11	0.50182816	0.40134710	0.49689944
B12	0.40013459	0.50055993	0.50235508
B13	0.50587253	0.73501794	0.16800923
B14	0.49492609	0.59873739	0.16550360
B15	0.59055934	0.49239894	0.16474640
B16	0.49658809	0.27431290	0.16865258
B17	0.49071770	0.49951291	0.26805094
B18	0.38641330	0.50171091	0.16692981
B19	0.48858997	0.49818555	0.06467602
B20	0.50270706	0.26388639	0.49831689
B21	0.59841731	0.15671908	0.50236411
B22	0.49893648	0.16921487	0.60326327
B23	0.50439075	0.84164617	0.26471606
B24	0.39996031	0.16423528	0.49963799
B25	0.15860080	0.50634492	0.26984244
B26	0.26432864	0.17372730	0.83852013
B27	0.05727321	0.50685512	0.82121445
B28	0.50086649	0.50044939	0.73542973
B29	0.39648125	0.50032019	0.83122557
B30	0.49749303	0.39764547	0.83582890
B31	0.60854917	0.83339138	0.16857230
B32	0.59799181	0.49713411	0.83902076
B33	0.50022488	0.59980341	0.83879881
B34	0.49555603	0.82951274	0.74120890
B35	0.39987769	0.82432860	0.84258850
B36	0.50312208	0.82813826	0.94171972
B37	0.59874287	0.83180634	0.83621324
B38	0.49648930	0.92976004	0.84372464
B39	0.16697620	0.26415834	0.50451081
B40	0.50824198	0.93585474	0.15572840
B41	0.84058052	0.15260719	0.73311295
B42	0.74219632	0.16356921	0.83716135
B43	0.83848669	0.05757870	0.83779893
B44	0.60315138	0.16807002	0.84342955
B45	0.15662251	0.50676764	0.06524653
B46	0.49871859	0.06908914	0.84495512
B47	0.15506988	0.40596026	0.82519891
B48	0.15665134	0.50790928	0.92536735
B49	0.25848883	0.50486904	0.82810631
B50	0.50032414	0.84467873	0.40160506
B51	0.15796029	0.60786551	0.82368584
B52	0.15767720	0.40653968	0.16837630
B53	0.16397595	0.83744476	0.73399954
B54	0.06646991	0.83582611	0.83501210

B55	0.50099307	0.17426912	0.94184269
B56	0.16568065	0.82352896	0.93195402
B57	0.26465923	0.82594453	0.83369604
B58	0.16904604	0.93094817	0.83974728
B59	0.05740879	0.50646883	0.16780993
B60	0.50210363	0.16809023	0.74222252
B61	0.40111593	0.17211215	0.84188380
B62	0.83863441	0.60298560	0.50193259
B63	0.49849564	0.74050289	0.49591915
B64	0.49679778	0.83368626	0.60293830
B65	0.06593218	0.16637160	0.49643630
B66	0.16672279	0.82538720	0.39946754
B67	0.60056438	0.84196034	0.50342461
B68	0.16426935	0.92964615	0.16544592
B69	0.16788128	0.82770474	0.26441516
B70	0.82733474	0.49729439	0.72451009
B71	0.73498280	0.49480220	0.83330137
B72	0.83935544	0.39616016	0.82470063
B73	0.84243097	0.49631526	0.92449760
B74	0.83273639	0.59735402	0.82501444
B75	0.16277353	0.16094757	0.59904007
B76	0.83863926	0.84151609	0.73493582
B77	0.73412901	0.83132144	0.82984837
B78	0.83490032	0.73364904	0.82812497
B79	0.82916669	0.82919134	0.93269905
B80	0.93263048	0.83247211	0.83747966
B81	0.16232418	0.06607835	0.49452185
B82	0.16797995	0.82519723	0.06659307
B83	0.06831863	0.82652678	0.16534352
B84	0.16461348	0.73352897	0.50669083
B85	0.26938964	0.83321303	0.16389399
B86	0.26427015	0.16193839	0.49974083
B87	0.49655205	0.94032491	0.50644153
B88	0.83038813	0.82847798	0.06709025
B89	0.73438852	0.15616149	0.49900659
B90	0.83647757	0.15908158	0.59653197
B91	0.93208801	0.16847063	0.49327350
B92	0.82804038	0.26414322	0.50265903
B93	0.16492016	0.83806920	0.59900730
B94	0.83909107	0.49272563	0.06271292
B95	0.73122087	0.48529177	0.16251376
B96	0.83823580	0.39080388	0.16247784
B97	0.83465357	0.49103221	0.26428743
B98	0.82556894	0.59069198	0.16445141
B99	0.16084261	0.17031528	0.07345240
B100	0.83963190	0.49954365	0.40146610
B101	0.73451884	0.50649565	0.49490772
B102	0.82916231	0.40132683	0.50274427

B103	0.26738831	0.83499701	0.49998521
B104	0.83148782	0.17047531	0.39576668
B105	0.16434110	0.26970589	0.17370046
B106	0.16442548	0.06800136	0.17139607
B107	0.94210874	0.16542832	0.16459995
B108	0.83048825	0.72782455	0.16643601
B109	0.83598271	0.83026341	0.26508371
B110	0.93266047	0.82399229	0.16423295
B111	0.83615879	0.92886607	0.16381946
B112	0.49662180	0.60259242	0.49466751
B113	0.26500245	0.16891032	0.16879926
B114	0.84024669	0.83657996	0.40037124
B115	0.74226750	0.84269374	0.50200692
B116	0.84282542	0.74141035	0.50561312
B117	0.84512968	0.84781873	0.59976181
B118	0.84379990	0.94240215	0.49491711
B119	0.16712001	0.16879929	0.27402655
B120	0.84618805	0.16488170	0.05753561
B121	0.74183309	0.17263019	0.15304542
B122	0.83811224	0.06622150	0.15944897
B123	0.83580754	0.16689155	0.25837467
B124	0.93202213	0.49801412	0.50916506
B125	0.84555851	0.25858004	0.82813919
B126	0.50668577	0.07478846	0.15561186
B127	0.40185189	0.16993649	0.16557194
B128	0.16286107	0.59911284	0.51020495
B129	0.26509295	0.50113903	0.50609138
B130	0.16700301	0.39963069	0.50693696
B131	0.50414798	0.16654674	0.26382835
B132	0.06630119	0.49770231	0.51310722
B133	0.16177254	0.60645164	0.16760147
B134	0.16501191	0.16319106	0.73604047
B135	0.17053057	0.06794437	0.84064607
C1	0.73944555	0.83071767	0.16760654
C2	0.49534385	0.07041172	0.50559746
C3	0.49556191	0.49909915	0.40182460
C4	0.40222441	0.83940826	0.50066736
C5	0.49998911	0.17999217	0.07068511
C6	0.48669588	0.40402253	0.16637548
C7	0.50170088	0.26533103	0.84002732
C8	0.49265798	0.49627040	0.93186903
C9	0.50194309	0.73305070	0.84275797
C10	0.07188784	0.16237553	0.83538976
C11	0.16309806	0.50399680	0.72947455
C12	0.92678733	0.49798028	0.16529635
C13	0.16146544	0.73796442	0.82613698
C14	0.07024254	0.83461804	0.49801801
C15	0.16700807	0.49943753	0.60343474

C16	0.16527509	0.16890983	0.40507069
C17	0.17039775	0.73587058	0.16646839
C18	0.50873946	0.82945228	0.07125525
C19	0.25270743	0.50333136	0.16687968
C20	0.07137218	0.16935090	0.17411182
C21	0.84649101	0.26090036	0.15857964
C22	0.83997962	0.07161803	0.49202394
C23	0.82853689	0.50123852	0.59468419
C24	0.94055275	0.83949412	0.49794876
C25	0.83431836	0.92693764	0.84028479
C26	0.92788596	0.50085482	0.81812736
C27	0.84640159	0.16331011	0.92744180
Na1	0.99934649	0.99626197	0.32201229
Na2	0.66731631	0.00061080	0.99831650
Na3	0.67036457	0.66841121	0.33793488
Na4	0.67920933	0.65846729	0.99763717
Na5	0.33435045	0.67127600	0.33779580
Na6	0.32810964	0.66829037	0.00003070
Na7	0.99526530	0.66255681	0.33698996
Na8	0.99137228	0.67303210	0.99821452
Na9	0.66634100	0.67239806	0.66142683
Na10	0.66565555	0.32694159	0.66166442
Na11	0.66145293	0.99941242	0.67328484
Na12	0.00763083	0.33998876	0.99428406
Na13	0.34267724	0.66848338	0.66166733
Na14	0.33760588	0.32455572	0.66072618
Na15	0.32863425	0.00317296	0.67813021
Na16	0.99250306	0.67858152	0.66632388
Na17	0.99596761	0.31746153	0.65760209
Na18	0.00953286	0.00164930	0.66957722
Na19	0.66970008	0.32737088	0.34145813
Na20	0.33142146	0.32532662	0.34388148
Na21	0.31313716	0.33141592	0.99692526
Na22	0.99951464	0.33885049	0.34935508
Na23	0.32595532	0.99983047	0.00008149
Na24	0.00687643	0.98432007	0.00604735
Na25	0.33433961	0.99925506	0.32154274
Na26	0.67900162	0.33534753	0.99318032
Na27	0.66606554	0.00495338	0.32726952

Table S7. Crystallographic data of the **1-Na-1C-2Crandom222** model (occupancy is 1 for all atoms).

Space group	*P1*
***a, b, c* (Å)**	8.1848
***α, β, γ* (°)**	90

Atom	***x***	***y***	***z***
B1	0.41178098	0.74584135	0.25821610
B2	0.11250925	0.24616120	0.74766357
B3	0.26269827	0.25224894	0.89677322
B4	0.41512868	0.24627215	0.74865854
B5	0.26179394	0.40086788	0.74473655
B6	0.25965865	0.74984185	0.10823417
B7	0.11089391	0.74616109	0.25939959
B8	0.25757343	0.75532429	0.41282312
B9	0.25925759	0.90105299	0.25769866
B10	0.73459851	0.41035805	0.24812460
B11	0.10159438	0.76003227	0.74809016
B12	0.25362899	0.60865870	0.74825900
B13	0.25260653	0.75482942	0.90108866
B14	0.39942741	0.76087529	0.74915950
B15	0.25209649	0.91135764	0.75004045
B16	0.73521636	0.25525409	0.09863692
B17	0.57942636	0.25986118	0.24856329
B18	0.26226978	0.24920642	0.59856044
B19	0.73492153	0.10761888	0.24918060
B20	0.75283284	0.23743707	0.59958593
B21	0.89800844	0.74889624	0.74532011
B22	0.74634150	0.74300648	0.89615955
B23	0.74646234	0.59298696	0.74818842
B24	0.59965055	0.74910554	0.74566100
B25	0.74723134	0.74280286	0.59890512
B26	0.75263193	0.89969075	0.24961435
B27	0.90231448	0.74726706	0.25170954
B28	0.75001666	0.75000487	0.39783285
B29	0.24157082	0.41034495	0.25184159
B30	0.74899545	0.74959753	0.09961520
B31	0.75203865	0.38547794	0.74876255
B32	0.90534628	0.23470431	0.74786554
B33	0.75189712	0.23739598	0.89733677
B34	0.75527719	0.08254988	0.74654119
B35	0.24209065	0.25606579	0.09925194
B36	0.08246085	0.25867970	0.25019613
B37	0.24029642	0.10702976	0.25006907
B38	0.24126893	0.25336737	0.39839760
B39	0.73601543	0.25526886	0.39867941
C1	0.74892680	0.88580020	0.74673386

C2	0.61087986	0.74640195	0.25059599
C3	0.26060705	0.60656171	0.25902262
C4	0.37931835	0.25982001	0.24875351
C5	0.87668155	0.25939105	0.24937921
C6	0.75082303	0.60844655	0.24818837
C7	0.25195165	0.75763502	0.60882206
C8	0.61219412	0.23408030	0.74882916
C9	0.26064060	0.10825117	0.74603597
Na1	0.49361886	0.99826489	0.00004762
Na2	0.49611609	0.49959622	0.97759224
Na3	0.50155359	0.00422092	0.49805845
Na4	0.00813391	0.49472529	0.97451200
Na5	0.00218938	0.48750429	0.52088059
Na6	0.00683051	0.99814724	0.99659052
Na7	0.50215472	0.49264660	0.51906378

Table S8. Crystallographic data of the **3-Na-1C-2Crandom333** model (occupancy is 1 for all atoms).

Space group	*P1*
***a, b, c* (Å)**	12.2772
***α, β, γ* (°)**	90

Atom	***x***	***y***	***z***
B1	0.16524991	0.93156059	0.49505602
B2	0.40757383	0.83562452	0.16256814
B3	0.15981314	0.17085158	0.93693295
B4	0.94188951	0.15698573	0.83343528
B5	0.16564610	0.49384992	0.40895530
B6	0.15949327	0.26863256	0.83169576
B7	0.60353065	0.18025049	0.16200234
B8	0.50033317	0.16044296	0.40258591
B9	0.59874965	0.50770937	0.49291071
B10	0.50399606	0.50101075	0.59806812
B11	0.50334607	0.40195296	0.49750796
B12	0.40088588	0.49804748	0.50423444
B13	0.50646023	0.73551224	0.16634911
B14	0.49558927	0.59955132	0.16527577
B15	0.59065981	0.49333014	0.16749953
B16	0.49692734	0.27452002	0.16983251
B17	0.49134433	0.50239560	0.26928012
B18	0.38722733	0.50177653	0.16684448
B19	0.49015459	0.49871612	0.06493379
B20	0.50356325	0.26403882	0.49883780
B21	0.59830113	0.15529174	0.50390477
B22	0.49815657	0.17086778	0.60498787

B23	0.50510260	0.84101280	0.26395572
B24	0.40009158	0.16803851	0.50160680
B25	0.15970139	0.50438427	0.27068677
B26	0.26390028	0.17443105	0.83897388
B27	0.05704489	0.50692548	0.82122800
B28	0.50070021	0.49882070	0.73543135
B29	0.39655943	0.50004250	0.83141434
B30	0.49628244	0.39780830	0.83570184
B31	0.60884861	0.83301436	0.16815358
B32	0.59763800	0.49724251	0.83875467
B33	0.50024500	0.60002560	0.83653813
B34	0.49735111	0.83332093	0.73252725
B35	0.40019430	0.82428582	0.83425610
B36	0.50266496	0.82936458	0.93510354
B37	0.59909987	0.83254454	0.82886372
B38	0.49692462	0.93126181	0.83734668
B39	0.50880223	0.93615500	0.15422522
B40	0.83973048	0.15357999	0.73417399
B41	0.74124720	0.16357098	0.83730860
B42	0.83678833	0.05787320	0.83790629
B43	0.60236433	0.16813260	0.84355916
B44	0.15470732	0.50777955	0.06584624
B45	0.49853729	0.07028516	0.84335970
B46	0.15471986	0.40550495	0.82712103
B47	0.15544760	0.50845039	0.92581782
B48	0.25829327	0.50422156	0.82879128
B49	0.50265226	0.84409173	0.40339949
B50	0.15753529	0.60732510	0.82339022
B51	0.15758748	0.40670141	0.16743860
B52	0.16199830	0.83637381	0.73453182
B53	0.06635913	0.83550513	0.83702435
B54	0.50070887	0.17439534	0.94227743
B55	0.16757163	0.82383087	0.93221782
B56	0.26468646	0.82587901	0.83143434
B57	0.16884772	0.93089122	0.83886168
B58	0.05753463	0.50681866	0.17111426
B59	0.50162656	0.17054636	0.74299745
B60	0.40047845	0.17352561	0.84266716
B61	0.83990829	0.60335507	0.49501647
B62	0.49741069	0.74125887	0.49971975
B63	0.06627685	0.16902133	0.49631321
B64	0.16905937	0.82486887	0.40085131
B65	0.60094145	0.84232337	0.50463553
B66	0.16448750	0.93012724	0.16706111
B67	0.16927915	0.82806106	0.26551802
B68	0.82745009	0.49683475	0.72120231
B69	0.73448053	0.49506413	0.83136521
B70	0.83887283	0.39635573	0.82425672

B71	0.84123747	0.49695644	0.92392552
B72	0.83297334	0.59746858	0.82337828
B73	0.16262965	0.16340329	0.60026243
B74	0.84050751	0.84165867	0.73549300
B75	0.73437645	0.83186131	0.82800541
B76	0.83499371	0.73374682	0.82774074
B77	0.82795242	0.82819593	0.93309465
B78	0.93249406	0.83242690	0.83983658
B79	0.16302905	0.06757093	0.49827652
B80	0.16839040	0.82589053	0.06735356
B81	0.06854967	0.82686746	0.16666859
B82	0.16560225	0.72984230	0.50674283
B83	0.26989442	0.83377939	0.16410936
B84	0.26473737	0.16600891	0.50073213
B85	0.49537173	0.94103686	0.50960752
B86	0.82994733	0.82684304	0.06776690
B87	0.73459307	0.15495619	0.50026168
B88	0.83660433	0.16047288	0.59785584
B89	0.93223886	0.17174381	0.49437922
B90	0.82652199	0.26449470	0.50141562
B91	0.16383553	0.83530683	0.60018343
B92	0.83746211	0.49357306	0.06454740
B93	0.73121885	0.48634200	0.16370612
B94	0.83866180	0.39148409	0.16531069
B95	0.82598984	0.59157267	0.16883721
B96	0.16109448	0.16980466	0.07466114
B97	0.83755503	0.49965033	0.39337299
B98	0.73386919	0.50900027	0.48814819
B99	0.82692961	0.40110186	0.49644109
B100	0.26803603	0.83382313	0.50392399
B101	0.83207399	0.16911897	0.39698300
B102	0.16449650	0.27043065	0.17395482
B103	0.16439586	0.06865978	0.17441877
B104	0.94213739	0.16616890	0.16568417
B105	0.82992728	0.72836962	0.17018708
B106	0.83449908	0.83185546	0.26625206
B107	0.93251661	0.82417150	0.16553623
B108	0.83612814	0.92891206	0.16289270
B109	0.49538517	0.60316732	0.49786688
B110	0.26541723	0.16970322	0.16946448
B111	0.83875450	0.83841142	0.40126313
B112	0.74282952	0.84298597	0.50512954
B113	0.84329630	0.74160301	0.50342680
B114	0.84664112	0.84703260	0.60072213
B115	0.84459230	0.94289095	0.49770370
B116	0.16775647	0.17159749	0.27510901
B117	0.84594016	0.16701270	0.05857039
B118	0.74172156	0.17331482	0.15451978

B119	0.83808249	0.06700713	0.15932009
B120	0.83610116	0.16619211	0.25996365
B121	0.93229327	0.49575860	0.50156277
B122	0.84482561	0.25890828	0.82932408
B123	0.50705124	0.07502093	0.15559917
B124	0.40223383	0.17042918	0.16616197
B125	0.16328186	0.59192413	0.50979420
B126	0.26616223	0.49318089	0.50826500
B127	0.16778968	0.39080893	0.50724554
B128	0.50393339	0.16547073	0.26492640
B129	0.06650133	0.49008772	0.51115238
B130	0.16220279	0.60682827	0.16922120
B131	0.16429257	0.16658890	0.73716767
B132	0.16958315	0.06814092	0.83966077
C1	0.16732816	0.25979067	0.50656141
C2	0.49933739	0.83600261	0.59905204
C3	0.83288468	0.49179992	0.26002906
C4	0.73931397	0.83051962	0.16851266
C5	0.49415225	0.07072544	0.50952126
C6	0.49559827	0.50237672	0.40268710
C7	0.40307191	0.84005602	0.50272379
C8	0.50022310	0.18033540	0.07144685
C9	0.48717195	0.40449016	0.16743839
C10	0.50019492	0.26613264	0.84107388
C11	0.49377275	0.49769703	0.93199580
C12	0.50192493	0.73343450	0.83622722
C13	0.07087430	0.16229073	0.83660276
C14	0.16300904	0.50028496	0.73011720
C15	0.92616995	0.49816178	0.16676065
C16	0.16128261	0.73759303	0.82634540
C17	0.07105214	0.83374678	0.49842892
C18	0.16676775	0.49210735	0.60405979
C19	0.16562697	0.16911747	0.40681292
C20	0.17093595	0.73633642	0.16764578
C21	0.50814061	0.83046761	0.06799603
C22	0.25249240	0.50332381	0.16677415
C23	0.07139971	0.17004383	0.17534046
C24	0.84628057	0.26195544	0.16245644
C25	0.84195714	0.07222922	0.49483381
C26	0.82925669	0.50064499	0.58785280
C27	0.94092486	0.83955334	0.49823502
C28	0.83361788	0.92687673	0.84031314
C29	0.92769257	0.50080106	0.81731492
C30	0.84593794	0.16478684	0.92857556
Na1	0.99441099	0.99251995	0.31943038
Na2	0.66523844	0.00004753	0.99085266
Na3	0.67458853	0.66394654	0.99465947
Na4	0.33787350	0.66819524	0.33607629

Na5	0.33075654	0.66876029	0.99775049
Na6	0.99835693	0.67073124	0.34030072
Na7	0.99402455	0.67751775	0.99540077
Na8	0.67299165	0.66723174	0.66064755
Na9	0.65948932	0.32216831	0.66353334
Na10	0.00933601	0.33686646	0.98967517
Na11	0.34038423	0.65549119	0.66584489
Na12	0.33330989	0.01466156	0.68677006
Na13	0.99122494	0.67852234	0.66700906
Na14	0.98733028	0.32065550	0.66437272
Na15	0.00319999	0.99917568	0.67621014
Na16	0.66158987	0.32089523	0.34843780
Na17	0.34251990	0.32866112	0.34317194
Na18	0.31711590	0.33219416	0.99045383
Na19	0.99812953	0.33525969	0.34740593
Na20	0.32880722	0.00057589	0.99698042
Na21	0.00522840	0.98367332	0.00468655
Na22	0.33966988	0.00003701	0.31385679
Na23	0.67318997	0.33169058	0.98802365
Na24	0.66840004	0.00405148	0.32731438

Table S9. Calculated ^{11}B and ^{23}Na NMR parameters in the NaB_5C structure (single cell) in which the B3 atom is in line with the C atom.

	δ_{iso} (ppm)	C_Q (MHz)	η
B1	5.4	1.74	0.56
B2	5.4	1.74	0.56
B3	12.3	0.44	0.00
B4	5.4	1.74	0.56
B5	5.4	1.74	0.56
Na	-15.2	-0.62	0.0

Table S10. Calculated ^{11}B NMR parameters in the $Na_8(B_5C)_8$ model **1Crandom222**.

	δ_{iso} (ppm)	C_Q (MHz)	η		δ_{iso} (ppm)	C_Q (MHz)	η
B1	3.3	-1.09	0.53	B21	7.1	-1.67	0.39
B2	-4.3	-1.55	0.21	B22	5.0	-1.73	0.59

B3	3.1	-1.75	0.50	B23	6.3	-1.71	0.55
B4	5.7	1.08	0.95	B24	13.1	-1.52	0.01
B5	19.7	-1.56	0.26	B25	5.8	-1.80	0.32
B6	-6.1	-1.59	0.38	B26	3.7	-1.63	0.59
B7	-7.1	-1.55	0.47	B27	12.7	-1.54	0.19
B8	7.3	-1.18	0.59	B28	8.7	-1.80	0.29
B9	8.5	-1.79	0.29	B29	5.9	-1.75	0.29
B10	14.7	-1.61	0.17	B30	2.8	-0.95	0.61
B11	5.3	-1.79	0.32	B31	7.0	-1.76	0.55
B12	4.5	-1.07	0.67	B32	4.5	-1.72	0.60
B13	-8.9	-1.59	0.25	B33	13.0	-1.57	0.14
B14	14.3	-1.62	0.02	B34	7.6	-1.71	0.38
B15	-4.7	-1.57	0.31	B35	6.5	-1.83	0.32
B16	4.4	-1.09	0.83	B36	1.1	-1.73	0.20
B17	5.5	-1.76	0.46	B37	16.0	-0.70	0.34
B18	16.4	-0.81	0.02	B38	-9.2	-1.52	0.55
B19	3.6	-1.80	0.21	B39	3.1	-1.74	0.38
B20	3.8	-1.70	0.62	B40	4.2	-1.71	0.46

Table S11. Calculated ^{11}B NMR parameters in the $Na_8(B_5C)_6(B_4C_2)(B_6)$ model **0C-2Crandom222**.

	δ_{iso} (ppm)	C_Q (MHz)	η		δ_{iso} (ppm)	C_Q (MHz)	η
B1	1.0	-0.72	0.78	B21	5.8	-1.61	0.47
B2	-4.8	-1.51	0.33	B22	4.0	-1.40	0.04
B3	3.4	-1.76	0.48	B23	3.1	-1.17	0.25
B4	6.8	-1.08	0.82	B24	8.6	-1.47	0.19
B5	19.0	-1.53	0.27	B25	7.8	-1.51	0.02
B6	-4.3	-1.70	0.36	B26	4.4	-1.23	0.11
B7	-9.7	-1.27	0.49	B27	16.1	-1.80	0.41

B8	9.1	-1.32	0.53	B28	16.1	-1.83	0.24
B9	9.1	-1.46	0.31	B29	12.5	-2.28	0.13
B10	14.1	-1.67	0.30	B30	2.9	-0.95	0.33
B11	3.8	-0.80	0.73	B31	10.7	-2.26	0.12
B12	5.2	-1.89	0.26	B32	8.7	-1.86	0.55
B13	-7.2	-1.47	0.39	B33	13.7	-1.43	0.02
B14	15.0	-1.47	0.11	B34	6.2	-1.65	0.44
B15	10.7	-1.95	0.23	B35	7.8	-1.94	0.20
B16	5.9	1.09	0.80	B36	1.5	-1.73	0.19
B17	5.1	-1.87	0.31	B37	16.1	-0.67	0.23
B18	15.2	-0.95	0.17	B38	-10.2	-1.49	0.75
B19	3.9	-1.81	0.22	B39	3.5	-1.75	0.38
B20	-9.3	-1.29	0.94	B40	4.1	-1.84	0.30

Table S12. Calculated ^{11}B NMR parameters in the $Na_{27}(B_5C)_{27}$ model **1Crandom333**.

	δ_{iso} (ppm)	C_Q (MHz)	η		δ_{iso} (ppm)	C_Q (MHz)	η		δ_{iso} (ppm)	C_Q (MHz)	η
B1	2.3	-1.84	0.18	B46	16.6	-1.58	0.12	B91	6.7	-1.73	0.23
B2	-5.6	-1.54	0.38	B47	-7.9	-1.56	0.45	B92	16.2	-1.56	0.11
B3	4.6	-1.55	0.10	B48	2.0	-1.36	0.03	B93	2.7	-1.80	0.54
B4	5.2	-1.18	0.20	B49	-10.9	-1.62	0.18	B94	4.1	-1.41	0.39
B5	6.1	-1.30	0.10	B50	4.8	-1.75	0.48	B95	13.4	-1.42	0.45
B6	5.5	-1.54	0.41	B51	4.3	-1.25	0.69	B96	5.5	-1.09	0.77
B7	5.2	-1.50	0.32	B52	-8.6	-1.58	0.18	B97	4.8	-1.66	0.27
B8	6.0	-1.71	0.52	B53	6.5	-1.71	0.28	B98	-5.1	-1.62	0.39
B9	5.9	-1.80	0.42	B54	6.6	-1.82	0.41	B99	-4.8	-1.46	0.20
B10	18.9	-1.54	0.30	B55	6.5	-1.13	0.58	B100	15.9	-1.54	0.10
B11	6.2	-1.70	0.23	B56	6.4	-1.66	0.52	B101	3.6	-1.80	0.32
B12	6.2	-1.79	0.37	B57	5.0	-1.65	0.35	B102	8.8	-1.66	0.17
B13	2.0	-1.62	0.35	B58	15.7	-1.56	0.06	B103	14.6	-0.69	0.24

B14	13.3	-1.77	0.12	B59	17.2	-1.01	0.25	B104	5.8	-1.61	0.51
B15	-5.2	-1.43	0.15	B60	-9.2	-1.53	0.39	B105	5.0	-1.61	0.39
B16	4.3	-1.02	0.70	B61	5.9	-1.71	0.28	B106	3.0	-1.66	0.30
B17	-5.4	-1.02	0.56	B62	6.7	-1.47	0.62	B107	3.5	-1.10	0.33
B18	3.4	-0.94	0.75	B63	-7.4	-1.51	0.55	B108	4.6	-1.64	0.26
B19	-5.6	-0.94	0.68	B64	3.9	-1.62	0.40	B109	5.5	-1.74	0.25
B20	16.5	-1.56	0.35	B65	4.6	-1.75	0.30	B110	17.8	-1.62	0.07
B21	5.4	-1.57	0.28	B66	2.3	-1.83	0.43	B111	5.0	-1.61	0.56
B22	5.3	-1.62	0.35	B67	19.2	-1.40	0.11	B112	7.0	-1.56	0.71
B23	16.2	-1.64	0.32	B68	17.7	-1.48	0.22	B113	15.2	-1.66	0.04
B24	4.3	-1.64	0.15	B69	5.5	-1.64	0.14	B114	4.5	-1.90	0.47
B25	3.7	-1.65	0.48	B70	5.8	-1.23	0.65	B115	8.3	-1.35	0.15
B26	18.2	-1.60	0.24	B71	15.8	-1.58	0.04	B116	-7.9	-1.55	0.54
B27	2.6	1.24	0.89	B72	5.9	-1.53	0.44	B117	4.0	-1.82	0.53
B28	16.2	-1.72	0.26	B73	-10.2	-1.43	0.33	B118	7.6	-1.33	0.92
B29	4.9	-1.66	0.23	B74	5.8	-1.73	0.17	B119	6.1	-1.12	0.70
B30	-2.2	-0.97	0.72	B75	19.6	-1.54	0.10	B120	4.5	-1.14	0.65
B31	5.9	-1.18	0.66	B76	6.1	-1.57	0.41	B121	-9.3	-1.42	0.59
B32	4.4	-1.74	0.58	B77	3.7	-1.81	0.47	B122	12.5	-1.65	0.22
B33	-2.2	-0.94	0.91	B78	17.4	-1.55	0.26	B123	-5.7	-1.60	0.35
B34	-6.0	-1.49	0.96	B79	6.2	-1.73	0.28	B124	2.5	-1.62	0.26
B35	3.3	-1.68	0.34	B80	4.7	-1.79	0.32	B125	-8.4	-1.52	0.59
B36	7.6	-1.18	0.28	B81	5.7	-1.70	0.40	B126	-9.6	-1.37	0.19
B37	6.0	-1.79	0.40	B82	5.9	-1.61	0.31	B127	5.7	-1.68	0.32
B38	15.5	-1.54	0.02	B83	4.1	-1.75	0.34	B128	6.9	-1.74	0.38
B39	5.4	-1.72	0.34	B84	2.7	-1.77	0.67	B129	3.5	-1.89	0.44
B40	3.3	-1.48	0.14	B85	5.1	-1.68	0.53	B130	6.5	-1.82	0.55
B41	15.3	-1.69	0.11	B86	3.5	-1.73	0.44	B131	16.3	-1.66	0.14
B42	-8.1	-1.46	0.50	B87	6.7	-1.17	0.45	B132	3.7	-1.72	0.40
B43	2.8	-1.18	0.38	B88	6.2	-1.71	0.37	B133	3.9	-1.13	0.70
B44	5.4	-1.54	0.64	B89	3.9	-1.66	0.26	B134	4.8	-1.68	0.38

B45	1.8	-1.54	0.45	B90	5.0	-1.61	0.32	B135	6.9	-1.72	0.31

Table S13. Calculated ^{11}B NMR parameters in the $Na_7(B_5C)7(B_4C_2)$ model **1-Na-1C-2Crandom222**.

	δ_{iso} (ppm)	C_Q (MHz)	η		δ_{iso} (ppm)	C_Q (MHz)	η
B1	-0.4	-0.67	0.84	B21	4.9	-1.74	0.21
B2	-3.7	-1.52	0.26	B22	0.9	-1.54	0.36
B3	1.9	-1.71	0.53	B23	17.7	-1.53	0.32
B4	4.6	-0.96	0.77	B24	3.6	-1.73	0.35
B5	17.1	-1.48	0.45	B25	4.9	-1.65	0.47
B6	-5.5	-1.66	0.35	B26	17.0	-1.94	0.55
B7	-8.6	-1.31	0.54	B27	19.4	-1.94	0.28
B8	9.8	-1.42	0.60	B28	10.3	-2.24	0.17
B9	14.8	-1.67	0.34	B29	2.1	-0.93	0.38
B10	1.4	-0.73	0.66	B30	6.9	-2.09	0.10
B11	4.4	-1.77	0.21	B31	-7.2	-1.45	0.73
B12	-10.6	-1.45	0.26	B32	14.7	-1.60	0.05
B13	16.8	-1.49	0.18	B33	4.0	-1.69	0.27
B14	4.8	-1.71	0.30	B34	7.3	-1.20	0.60
B15	6.3	1.08	0.95	B35	-0.2	-1.68	0.23
B16	3.7	-1.82	0.33	B36	16.8	-0.71	0.25
B17	14.4	-0.91	0.18	B37	-9.4	-1.53	0.75
B18	5.3	-1.84	0.17	B38	5.0	-1.81	0.37
B19	-7.2	-1.33	0.92	B39	5.0	-1.86	0.26
B20	6.4	-1.74	0.38				

Table S14. Calculated ^{11}B NMR parameters in the $Na_{24}(B_5C)_{24}(B_4C_2)_3$ model **3-Na-1C-2Crandom333**.

	δ_{iso} (ppm)	C_Q (MHz)	η		δ_{iso} (ppm)	C_Q (MHz)	η		δ_{iso} (ppm)	C_Q (MHz)	η

B1	-1.7	-1.61	0.15	B45	16.8	-1.51	0.18	B89	-1.0	-1.45	0.36
B2	-6.9	-1.52	0.43	B46	-6.5	-1.59	0.29	B90	15.4	-1.56	0.07
B3	5.1	-1.49	0.08	B47	1.5	-1.29	0.09	B91	3.3	-1.89	0.36
B4	4.1	-1.12	0.17	B48	-9.1	-1.66	0.18	B92	17.9	-1.71	0.11
B5	3.9	-1.35	0.05	B49	17.6	-2.06	0.35	B93	17.5	-1.87	0.50
B6	7.2	-1.64	0.45	B50	3.8	-1.24	0.93	B94	3.1	-1.47	0.13
B7	5.2	-1.47	0.35	B51	-7.3	-1.58	0.20	B95	-3.5	-2.05	0.14
B8	1.2	-1.61	0.65	B52	7.0	-1.70	0.25	B96	-1.1	-1.54	0.11
B9	7.1	-1.78	0.30	B53	7.6	-1.83	0.40	B97	13.1	-0.45	0.49
B10	19.3	-1.61	0.19	B54	3.6	-0.97	0.80	B98	5.6	-2.00	0.34
B11	8.6	-1.72	0.42	B55	5.1	-1.64	0.57	B99	5.8	-1.66	0.17
B12	5.5	-1.76	0.43	B56	4.5	-1.65	0.37	B100	12.0	-0.51	0.64
B13	4.4	-1.70	0.44	B57	15.3	-1.56	0.06	B101	4.2	-1.55	0.48
B14	15.7	-1.85	0.18	B58	12.7	-0.65	0.53	B102	5.4	-1.67	0.37
B15	-7.2	-1.21	0.25	B59	-5.0	-1.63	0.27	B103	2.8	-1.70	0.22
B16	3.7	-0.98	0.81	B60	5.6	-1.67	0.22	B104	4.4	-1.11	0.47
B17	-4.8	-1.20	0.63	B61	6.0	-1.55	0.68	B105	1.7	-1.44	0.24
B18	3.3	-0.83	0.75	B62	-5.9	-1.94	0.18	B106	7.4	-1.79	0.18
B19	-6.0	-1.03	0.53	B63	3.9	-2.06	0.18	B107	17.1	-1.56	0.02
B20	19.7	-1.56	0.24	B64	1.1	-1.86	0.41	B108	4.4	-1.52	0.57
B21	9.2	-1.62	0.24	B65	24.4	-1.99	0.04	B109	2.4	-1.39	0.73
B22	11.4	-1.88	0.28	B66	17.5	-1.45	0.23	B110	17.5	-1.75	0.03
B23	13.9	-1.35	0.45	B67	4.7	-1.60	0.11	B111	5.3	-1.96	0.60
B24	0.6	-1.48	0.39	B68	8.1	-1.10	0.73	B112	8.8	-1.22	0.26
B25	2.8	-1.67	0.39	B69	17.5	-1.69	0.05	B113	-6.8	-1.53	0.56
B26	22.0	-1.75	0.20	B70	6.2	-1.62	0.31	B114	4.2	-1.92	0.43
B27	1.2	1.20	0.82	B71	-12.8	-1.17	0.51	B115	7.7	1.35	0.95
B28	18.8	-1.78	0.19	B72	7.0	-1.80	0.05	B116	2.4	0.90	0.79
B29	6.3	-1.65	0.38	B73	20.6	-2.05	0.02	B117	4.3	-1.29	0.79
B30	-0.8	-1.12	0.75	B74	8.6	-1.63	0.34	B118	-8.2	-1.50	0.61
B31	8.4	-1.34	0.79	B75	6.0	-1.82	0.36	B119	16.1	-1.68	0.19

B32	2.4	-1.67	0.53	B76	16.0	-1.47	0.23	B120	-5.9	-1.69	0.36
B33	-3.2	0.94	0.96	B77	3.4	-1.67	0.37	B121	-2.3	-1.55	0.38
B34	-3.2	1.41	0.13	B78	2.3	-1.69	0.41	B122	-9.6	-1.44	0.55
B35	1.2	-1.66	0.21	B79	16.8	-1.96	0.25	B123	-9.6	-1.37	0.11
B36	0.2	-1.00	0.30	B80	6.1	-1.61	0.37	B124	5.3	-1.62	0.29
B37	7.3	-1.92	0.37	B81	3.6	-1.76	0.30	B125	-3.2	-1.46	0.49
B38	17.2	-1.70	0.05	B82	5.0	-1.66	0.78	B126	5.7	-2.02	0.29
B39	2.3	-1.47	0.22	B83	6.0	-1.72	0.54	B127	3.8	1.05	0.75
B40	17.7	-1.74	0.11	B84	6.3	-2.17	0.19	B128	15.9	-1.65	0.19
B41	-6.2	-1.55	0.59	B85	5.3	-1.56	0.21	B129	0.4	-1.73	0.40
B42	4.3	-1.28	0.57	B86	3.4	-1.70	0.30	B130	4.0	-1.16	0.57
B43	5.5	-1.55	0.75	B87	10.2	-1.78	0.22	B131	1.0	-1.47	0.53
B44	1.8	-1.57	0.55	B88	7.4	-1.72	0.24	B132	5.1	-1.70	0.23

Table S15. Calculated ^{23}Na NMR parameters in the $Na_8(B_5C)_8$ model **1Crandom222**, $Na_8(B_5C)_6(B_4C_2)(B_6)$ model **0C-2Crandom222** and $Na_7(B_5C)_7(B_4C_2)$ model **1-Na-1C-2Crandom222**.

	1Crandom222			**0C-2Crandom222**			**1-Na-1C-2Crandom222**		
	δ_{iso} (ppm)	C_Q (MHz)	η	δ_{iso} (ppm)	C_Q (MHz)	η	δ_{iso} (ppm)	C_Q (MHz)	η
Na1	-11.9	0.70	0.77	-10.2	1.07	0.11	-12.1	-0.92	0.31
Na2	-11.7	0.81	0.33	-4.6	1.23	0.39	-6.7	1.01	0.11
Na3	-9.2	0.58	0.16	-8.4	0.93	0.77	-11.1	-0.69	0.38
Na4	-12.7	0.47	0.92	-8.4	1.01	0.73	-11.3	0.69	0.93
Na5	-11.6	0.89	0.46	-7.4	-1.09	0.79	-10.7	-0.82	0.85
Na6	-13.2	0.47	0.55	-12.7	0.76	0.61	-13.5	0.51	0.92
Na7	-12.3	0.91	0.49	-11.7	1.05	0.61	-6.1	0.88	0.46
Na8	-9.1	0.73	0.41	-3.0	-1.09	0.93			

Table S16. Calculated ^{23}Na NMR parameters in the $Na_{27}(B_5C)_{27}$ model **1Crandom333** and $Na_{24}(B_5C)_{24}(B_4C_2)_3$ model **3Na-1C-2Crandom333.**

	1Crandom333			**3Na-1C-2Crandom333**		
	δ_{iso} (ppm)	C_Q (MHz)	η	δ_{iso} (ppm)	C_Q (MHz)	η
Na1	-11.4	0.48	0.30	-9.4	0.43	0.80
Na2	-11.3	-0.47	0.48	-11.3	-0.46	0.29
Na3	-15.4	0.57	0.76	-13.9	0.53	0.86
Na4	-11.8	-0.36	0.02	-14.2	0.81	0.51
Na5	-13.7	0.53	0.60	-12.6	0.58	0.93
Na6	-11.3	-0.55	0.58	-9.4	1.17	0.06
Na7	-11.3	0.85	0.08	-7.3	-0.88	0.76
Na8	-8.9	-0.66	0.45	-15.0	-0.82	0.89
Na9	-14.9	0.55	0.79	-12.8	-0.52	0.87
Na10	-14.5	-0.47	0.87	-7.6	-0.33	0.55
Na11	-13.6	-0.48	0.32	-10.4	1.18	0.47
Na12	-8.6	-0.43	0.61	-9.9	-0.49	0.65
Na13	-11.4	-0.50	0.72	-7.5	0.69	0.79
Na14	-12.3	0.41	0.27	-6.3	0.79	0.14
Na15	-14.5	0.25	0.51	-8.2	0.75	0.65
Na16	-7.6	0.75	0.87	-6.5	-0.54	0.09
Na17	-6.3	0.57	0.67	-10.9	1.07	0.21
Na18	-8.0	0.74	0.12	-10.6	0.51	0.86
Na19	-11.1	0.55	0.59	-8.0	1.47	0.45
Na20	-12.8	0.57	0.28	-13.9	-0.41	0.90
Na21	-10.3	0.62	0.40	-9.5	-0.55	0.56
Na22	-9.5	0.56	0.81	-9.5	0.59	0.74
Na23	-13.4	-0.33	0.53	-9.5	0.99	0.35
Na24	-9.3	-0.57	0.60	-13.7	0.44	0.40
Na25	-13.0	0.23	0.14			
Na26	-7.9	1.27	0.16			
Na27	-13.6	0.38	0.78			